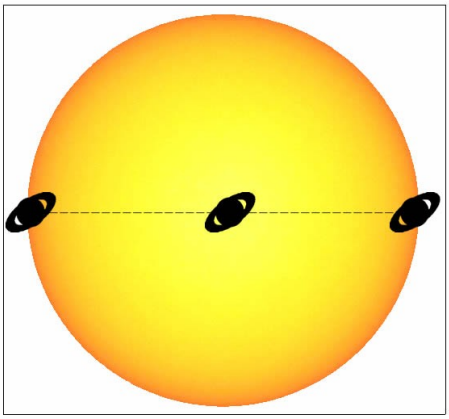

Detecting rings around exoplanets

Akinbowale Babatunde Akinsanmi
Mestrado em Astronomia
Departamento de Física e Astronomia
2017

Orientador
Nuno C. Santos,
Professor Auxiliar, Faculdade de Ciências da Universidade do Porto.

Coorientador
Mahmoudreza Oshagh
Investigador, Centro de Astrofísica, Universidade do Porto and
Institut für Astrophysik, Georg - August - Universität Göttingen.

Susana C.C. Barros
Investigador, Centro de Astrofísica, Universidade do Porto.

U.PORTO

FACULDADE DE CIÊNCIAS
UNIVERSIDADE DO PORTO

Todas as correções determinadas pelo júri, e só essas, foram efetuadas.

Pedro Viana

Porto, 20 / 07 / 2017

Faculdade de Ciências da Universidade

do Porto

Departamento de Física e Astronomia

Detecting Rings Around Exoplanets

Master in Astronomy Dissertation

Author:

Akinbowale Babatunde AKINSANMI[1,2]

Supervisors:

Nuno C. SANTOS[1,2]

Mahmoudreza OSHAGH[1,3]

Susana C.C. BARROS[1]

Affiliations:

[1] Centro de Astrofísica, Universidade do Porto, Rua das Estrelas, 4150-762 Porto, Portugal.

[2] Departamento de Física e Astronomia, Faculdade de Ciências, Universidade do Porto, Rua do Campo Alegre, 4169-007 Porto,Portugal

[3] Institut für Astrophysik, Georg - August - Universität Göttingen, Friedrich-Hund-Platz 1, 37077 Göttingen, Germany.

Acknowledgements

My sincere gratitude goes to my supervisors for their support, advice and also commitment towards my development. It was only by standing on their shoulders I was able to see farther and complete the work for this thesis.

To my mother, thank you for your encouragement and consistent belief in me which helped me through very challenging times and made me more resolute. My gratitude goes also to my siblings and girlfriend for their patience and support in various ways.

I thank also my astronomy colleagues for the enlightening discussions and for making my study in Portugal an interesting one. To my other friends in Porto, thank you for being my family here and helping me settle in comfortably.

My appreciation extends to the Director of ESS NASRDA, and the Heads of my department and team for opportunity granted me to pursue my Masters degree.

I express gratitude to the EXOEARTHS team and the entire CAUP for creating an enabling environment that motivated me, helped increase my curiosity and brought clarity to a lot of doubts.

Finally, I acknowledge the support of Fundação para a Ciência e a Tecnologia (FCT) (project ref. PTDC/FIS-AST/1526/2014) through national funds and by FEDER through COMPETE2020 (ref. POCI-01-0145-FEDER-016886), as well as through grant UID/FIS/04434/2013 (POCI-01-0145-FEDER-007672).

Abstract

It is theoretically possible for rings to have formed around extrasolar planets like they formed around the giant planets in our Solar system. However, no such rings have been detected till date. Planetary transits offer very valuable information about the properties of planets. Thus, the possibility of detecting rings around exoplanets can be probed by investigating possible ring signatures in high-precision photometric and spectroscopic transit signals. The transit signals of a ringed planet are expected to show deviations from those of a spherical planet and these deviations can be used to quantify the detectability of rings.

In this thesis, a numerical planet transit tool was modified to include the effects of planetary rings. The new tool is tested, validated and employed to simulate the photometric and spectroscopic transit of ringed planets. The tool is applied to measure ring detectability based on amplitudes of the residuals between the ringed planet signal and best fit of a ringless model. The detectability of rings is assessed for different possible ring orientations. The work also investigates the precision required for ring detection and the prospects of upcoming instruments like *ESPRESSO*@VLT and *CHEOPS* in the detection of exoplanetary rings.

Keywords: technique: photometric, radial velocities - methods: Numerical, analytical -planets and satellites: rings

Resumo

É teoricamente possível que os anéis se tenham formado em torno de planetas extrasolares, como se formaram em torno dos planetas gigantes no nosso sistema solar. No entanto, nenhum desses anéis foi detectado até a data. Os trânsitos planetários oferecem informações muito valiosas sobre as propriedades dos planetas. Assim, a possibilidade de detectar anéis em torno de exoplanetas pode ser avaliada investigando possíveis assinaturas de anéis em sinais fotométricos e espectroscópicos de alta precisão em trânsitos. Espera-se que os sinais de trânsito de um planeta com anéis mostrem desvios quando comparado com os de um planeta esférico e esses desvios podem ser usados para quantificar a detectabilidade dos anéis.

Nesta tese, uma ferramenta de trânsito do planeta numérico foi modificada para incluir os efeitos de anéis planetários. A nova ferramenta é testada, validada e empregada para simular o trânsito fotométrico e espectroscópico de planetas com anel. A ferramenta é aplicada para medir a detectabilidade do anel com base na amplitude dos resíduos entre o sinal do planeta com anéis e o modelo sem anel. A detectabilidade dos anéis é avaliada para diferentes possíveis orientações do anel. O trabalho também investiga a precisão necessária para a detecção de anéis e as perspectivas de instrumentos futuros como *ESPRESSO*@VLT e *CHEOPS* na detecção de anéis exoplanetários.

Contents

List of Figures

List of Tables

Chapter 1

Introduction

1.1 Context

The discovery of the first planet orbiting a Sun-like star, 51 Pegasi, marked an important milestone in Astronomy and our understanding of planetary systems. The planet (51 Peg b) was announced to have a mass of 0.5 M_{Jup} with an orbital period of only 4.23 days (Mayor and Queloz, 1995). This discovery of a gas giant planet so close to its star challenged the Solar System model and showed that planetary systems can be diverse. This fueled the detection of more exoplanets and since then, the number of confirmed exoplanets has increased to over 3000[1].

Exoplanets are discovered using different observational techniques (Perryman, 2011), the most successful of which are the radial velocity (RV) and transit techniques. The transit technique searches for dips in the brightness of a star caused by the passage of a planet across the disk of a star. It is especially useful in deducing the planet-star radius ratio[2]. The RV technique measures the star's line-of sight motion about the center of mass due to the presence of an orbiting planet. The doppler shift of spectral lines due to the star's radial motion leads to a periodic signal whose amplitude is related to the minimum mass of the planet relative to the stellar mass. For a rotating star, the transit of a planet blocks stellar regions with different radial velocity (RV) components thereby causing a RV anomaly called the Rossiter McLauglin (RM) effect.

[1] http://exoplanets.eu/

[2] If the stellar radius is known then the planet radius can be easily determined

The detected exoplanets vary in mass, radius and orbital properties proving that planetary systems are very diverse. There is therefore an ever growing need for detailed characterisation of exoplanets by constraining and detecting new properties such as planet's composition and internal structure, atmospheric and cloud composition, oblateness, day-night temperature difference, satellites e.t.c. A combination of techniques can be used to constrain the properties of a planet e.g. for a planet observed with the radial velocity and transit techniques, the planet's density can be computed and this provides useful constraint on its composition.

Planetary rings are unique features in our Solar System yet to be detected around extrasolar planets. The giants planets in our Solar System all have rings with different radial extents and particle size. Just as the planets in our Solar System motivated the search for exoplanets, the rings of the giant planets have raised questions on the existence of rings around exoplanets (Brown et al., 2001; Schlichting and Chang, 2011; Kenworthy and Mamajek, 2015). There is no reason to exempt the formation of rings around exoplanets especially beyond the ice line and so several studies are being conducted in order to detect this elusive structure. An interesting discovery of a giant ring-like structure extending up to 0.6 Au around an unseen stellar companion J1407b was reported by Mamajek et al. (2012) and Kenworthy and Mamajek (2015). However, the ring-like structure could either be a circumstellar disk or circumplanetary disk depending on true nature of J1407b, whether it is a brown dwarf or a giant planet.

The detection of exoplanetary rings would have tremendous astronomical implications and could usher a paradigm shift in our understanding of planetary formation and evolution. For instance, detecting rings around short-period giant planets, similar or dissimilar to those in our solar system, would require novel explanations as to how/where the planet and ring formed (in-situ or by migration). Depending on the distance from the star where a ringed planet forms, the composition of its rings would differ. The detection of a close-in ringed planet would imply it probably formed close

to that location since the icy rings of an initially long-period ringed planet would have sublimed if it migrated inwards.

Detection of planetary rings could also offer a way to detect the planetary spin axis of exoplanets if we assume that the ring axis is aligned with the planetary spin as we have in our Solar System. Additionally, if rings are found around several exoplanets, ensemble studies can be used to gain insight into their formation/lifetime by comparing frequency of rings with stellar age (Barnes and Fortney, 2004). If rings are found to be independent of stellar age, it could imply that they are long lived, constantly replenished or easily formed at any epoch. It could also imply that they are formed during planet formation and persist for a long time. However, if they are only found around planets orbiting old stars it implies that they are formed by later events. Conversely, if found only around planets orbiting young stars, it would imply that ring structures decay with time and are not replenished. This is of course dependent on how precisely we can measure stellar ages (Soderblom, 2010).

The rings of both Uranus and Neptune were detected as the planets occulted background stars (Elliot et al., 1978; Hubbard et al., 1985). The technique of stellar occultation can also be used to detect rings around exoplanets by monitoring changes in the stellar brightness as the planet transits its host star. Schneider (1999) was the first to propose that the transit of a planet with significantly opaque rings would cause distortions to the transit light-curve observed relative to that of a spherical planet by causing dips in the light curve before and after the planet transits. These distortions will also be observed in the RM signal for spectroscopic transit measurements (Ohta et al., 2009).

Barnes and Fortney (2004) showed that photometric precision of $100-300$ ppm with 15 minute time resolution would suffice for the detection of Saturn-like rings around a transiting exoplanet. Zuluaga et al. (2015) presented a large-scale photometric transit survey method to identify ringed planet candidates. The method uses the anomalously

large transit depth and anomalous estimation of transit derived stellar density to probe the presence of a ring. In addition, the photometric search for rings using real data has also been performed. Heising et al. (2015) searched for ringed planets around 21 short-period planets in *Kepler* photometry and found no evidence for rings. Aizawa et al. (2017) also searched for rings in *Kepler* photometry around 89 long-period planet candidates that exhibit transit-like signals. They found a planet candidate with orbital period of 450 years whose transit signal could be explained by one of three scenarios: the presence of a planetary ring, a circumstellar disk or a hierarchical triple. Lecavelier des Etangs et al. (2017) searched for transit signature of satellites and rings around the long-period planet CoRoT-9b and excluded the presence of both bodies around the planet.

In addition to the photometric techniques to detect rings, Ohta et al. (2009) studied complementary spectroscopic detection using the RM effect. They concluded that rings could be detected with radial velocity precision of 1 m/s if not viewed close to edge-on.

1.2 Objectives

The objective of this thesis was to contribute to the understanding of how planetary rings can be detected around exoplanets. In particular, it is to investigate the detectability of different ring orientations in high-precision transit photometry and radial velocity and to assess the prospect of upcoming observing instruments for ring detection.

The work involved contributing to the development of a ringed planet transit tool by modifying the existing planet transit tool SOAP2.0-T (Oshagh et al., 2016). The new tool (SOAP3.0) is used to simulate the photometric and spectroscopic transit of a ringed planet and is capable of delivering the expected light-curve and RM signal for ringed planet transits.

1.3 Dissertation structure

Chapter 2 describes the theory of planetary transits and how the useful parameters extracted from their analyses are employed in the detection and characterisation of exoplanets. It also gives a brief theoretical background of ring systems and the constraints for rings around exoplanets. Chapter 3 describes the developments that lead to the numerical tool (SOAP3.0) used in simulating ringed planet transits. The input and output parameters of the tool are explained and the tool is validated by comparing its results with those in literature. In Chapter 4, the tool is applied to investigate the detectability of different ring orientations in high-precision transit photometry and radial velocity. Chapter 5 discusses the factors that can influence the transit signal of a ringed planet and also the ring signature. It also discusses the prospects of upcoming state-of-the-art instruments for detecting rings. Finally, in Chapter 6 some conclusions are drawn based on the results achieved and possible future work is mentioned.

Chapter 2

Planetary Transits and Rings

The planetary transit method for the detection and characterisation of exoplanets offers a wealth of information about planets which are not accessible through the other planet detection techniques. These details are obtained from intricate observations of the combined light from the star and planet. Two observational techniques are employed to extract valuable information from transits: Photometry and spectroscopy. The photometric and spectroscopic transit techniques allow for the characterisation of properties such as planetary radius, orbital inclination and velocity of stellar rotation amongst others. These transit techniques have been applied in the detection of multi-planetary systems (Gillon et al., 2017), study of planet oblateness (Carter and Winn, 2010a; Carter and Winn, 2010b; Zhu et al., 2014), investigation of exoplanetary atmospheres using transmission and occultation spectroscopy (Charbonneau et al., 2002; Deming et al., 2005; Madhusudhan et al., 2014) and also in the measurement of spin-orbit misalignment (Sanchis-Ojeda and Winn, 2011; Addison et al., 2016).

2.1 Photometric transit

Photometry is used to measure the amount of light coming from astronomical bodies. The photometric transit technique has been used to detect a large number of the exoplanets known today. The transit of a planet across its host star causes a dimming of the stellar flux as part of it is blocked out by the planet. A light-curve is produced from the measurement of the flux as a function of time as depicted in Figure 2.1a. The

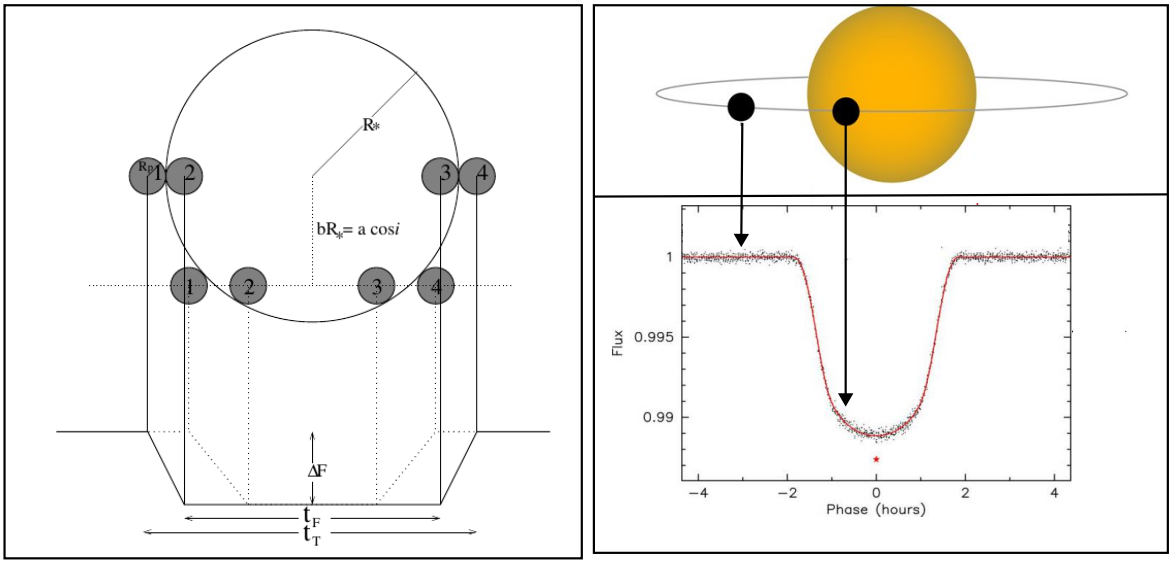

(A) (B)

FIGURE 2.1: (A) Geometry of planetary transit showing the four contact points for different impact parameter (b) transits. The produced light-curves are shown at the bottom with the observables labeled (Seager and Mallén-Ornelas, 2003). (B) Illustration of the orbit of a planet around limb darkened star. The light-curve of *Kepler-51 b* (Endl et al., 2011) is shown with arrows depicting flux measurement at different points in planet orbit. A flux dimming is noticed during the transit of the planet across the star.

observables from a transit light curve are: The depth of transit ΔF, the total transit duration t_T (contacts 1 to 4) and duration of complete transit t_F (contacts 2 to 3). If more than one transit is observed, the orbital period P of the planet can also be determined. With these, it is possible to infer and derive several parameters of the system.

2.1.1 Deriving parameters from Light-curve observables

The depth of the transit is related to the area of stellar disc covered by the planet allowing us to obtain the planet-star radius ratio. In the simple case of a planet on circular orbit around a uniform intensity star, the transit depth is given by

$$\Delta F \simeq \frac{R_p^2}{R_*^2} \quad , \tag{2.1}$$

where R_p and R_* are the radii of the planet and star respectively. Therefore, it will be easier to detect a planet with large radius or around smaller star since a greater flux dimming would be produced. As seen in Figure 2.1a, the duration of transit is affected by the impact parameter b defined as the sky-projected distance between the centers of the planet and stellar disc at midtransit. The value of b and scaled semi-major axis a/R_* can be derived from the transit observables as shown in Seager and Mallén-Ornelas (2003) for a circular orbit as

$$b = \frac{a}{R_*}\cos i_p = \left\{ \frac{(1-\sqrt{\Delta}F)^2 - \frac{\sin^2(t_F\pi/P)}{\sin^2(t_T\pi/P)}(1+\sqrt{\Delta}F)^2}{[1-\sin^2(t_F\pi/P)/\sin^2(t_T\pi/P)]} \right\}^{1/2}, \tag{2.2}$$

where i_p is the inclination of the planet's orbit and can be calculated since the ratio of a/R_* is derived as

$$\frac{a}{R_*} = \left\{ \frac{(1+\sqrt{\Delta}F)^2 - b^2[1-\sin^2(t_T\pi/P)]}{\sin^2(t_T\pi/P)} \right\}^{1/2}. \tag{2.3}$$

Kepler's third law for a circular orbit is

$$P^2 = \frac{4\pi^2 a^3}{G(M_* + M_p)}, \tag{2.4}$$

where G is the gravitational constant. With the reasonable approximation that the planet mass M_p is very small compared to the stellar mass M_*, equations 2.2 - 2.4 can be combined to derive the stellar density as

$$\rho_* \equiv \frac{M_*}{R_*^3} = \left[\frac{4\pi^2}{P^2 G}\right]\left\{\frac{a}{R_*}\right\}^3. \tag{2.5}$$

It is evident that a lot can be inferred from a transit light-curve. However, transits are only observable for certain impact parameters. For a transit to occur, b must satisfy $|b| < 1 \pm R_p/R_*$. The geometric probability that a randomly oriented planet

will transit its host star is given (e.g by Perryman 2011) as

$$Prob_{tr} = \left(\frac{R_* \pm R_p}{a}\right)\left(\frac{1}{1-e^2}\right) \tag{2.6}$$

where e is the eccentricity of the orbit and is equal to zero for the simple circular orbit considered in our formulation. The "+" or "-" sign allows for grazing transits or excludes them. Therefore, it will be more likely to observe transits for close-in planets or planets with eccentric orbits.

2.1.2 Limb Darkening

In reality stars do not have a uniform intensity, their discs are brighter at the center and darker towards the limb. This is intuitively referred to as limb darkening and is as a result of variations in the stellar atmospheric density and temperature with altitude. The line of sight to the limb is more oblique than it is towards the center causing an optical depth of unity to be attained at high stellar altitude where the density, temperature and intensity are lower.

Limb darkening causes a greater transit depth at the center than regions towards the stellar limb therefore the bottom of the light-curve will not appear flat as shown in Fig. 2.1a. The transit across a limb darkened star is illustrated in Fig. 2.1b where a more rounded light-curve is observed. To account for limb darkening effects in light-curves, several limb darkening models have been proposed, one of which is the widely adopted quadratic limb darkening model which allows for good transit computations (Mandel and Agol, 2002). The model is defined by two limb darkening coefficients u_1 and u_2 such that the normalized stellar intensity is a function of normalized radial distance r from the center of the disc and given by

$$I(r) = 1 - u_1(1-\mu) - u_2(1-\mu)^2, \qquad u_1 + u_2 \leq 1 \tag{2.7}$$

and $r = \sqrt{\frac{x^2+y^2}{R_*^2}}$

where x and y represent co-ordinates centered on the stellar disk in sky plane XY. Thus, we must have $r = 0$ at center of stellar disk and $r = 1$ on the stellar limb. μ is the directional cosine defined by the angle θ between line of sight of observer and the normal to stellar surface and it is given by: $\mu = \cos\theta = \sqrt{1 - r^2}$. The specific intensity $I(r)$ at the center of star is $I(0) = 1$ and reduces towards the stellar limb.

2.2 Spectroscopic transit

In addition to the photometric signal of a transiting planet, a spectroscopic transit signal can be obtained from the measurement of the star's radial velocity shift during planetary transit. When a star is rotating, half of the stellar disc rotates towards the observer while the other half rotates away from the observer. Due to Doppler effect, light from the approaching half will appear blue-shifted while light from the receding half will appear red-shifted (see Fig. 2.2). Outside of transit, the rotation causes the spectral lines to be broadened but this does not lead to an overall doppler shift since the effect from both halves of stellar disc will average out when integrated. However, when a planet transits the star, it blocks part of the blueshifted half causing the integrated stellar light to be slightly redshifted. The same happens when it blocks part of the redshifted half leading to a slightly blueshifted integrated stellar light.

As the planet transits across the stellar disc, it covers different regions with varying radial velocity components thereby causing a RV anomaly referred to as the Rossiter-McLaughlin (RM) effect (Rossiter, 1924; McLaughlin, 1924). Fig. 2.2 illustrates the RM signals for a planet with same parameters but following different paths across the star. The three paths would produce the same light-curve but different RM signals. The RM effect is useful in the measurement of the spin-orbit misalignment angle λ and projected stellar rotational velocity $\nu \sin i_*$. As seen, the RM signal of the well-aligned planet (λ=0°) is anti-symmetric about the midtransit time whereas that of the misaligned planets will either be asymmetric (λ=30°) or produce the anomaly from only

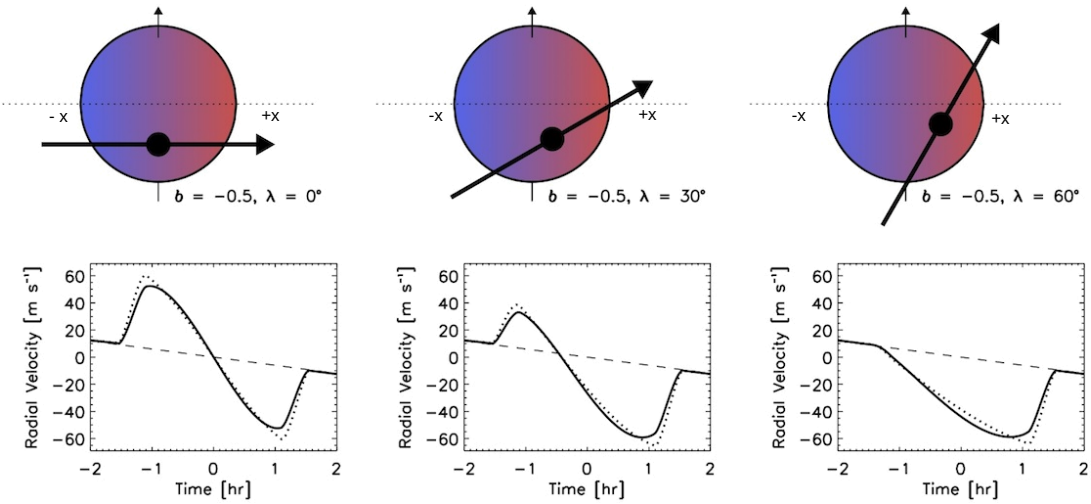

FIGURE 2.2: Top: Transits of a planet across a rotating star with three different paths (defined by angle λ between projected planet orbit and stellar spin axis). Bottom: The different RM signals produced by the three planet orbit paths. The long dashed line shows the star's RV without a transiting planet. Solid and dotted curves show the RM signals with and without limb darkening. From Gaudi and Winn (2007).

one of the hemispheres (λ=60°).

The radial velocity anomaly due to the RM effect $\Delta\nu_{RM}$ is given (for instance by Ohta et al. 2005) as

$$\Delta\nu_{RM} = -\nu \sin i_* \frac{\int\int x\, I(r)\, dx\, dy}{\int\int I(r)\, dx\, dy}, \qquad r(x,y) \tag{2.8}$$

This shows that the RM effect depends on the position on the x axis. The star is centered at x=0, so for the negative x values corresponding to the blueshifted part of the star, a positive radial velocity anomaly (RM) will be observed and vice-versa. The RM effect is also proportional to the projected stellar rotational velocity $\nu \sin i_*$ so for a fast rotating star, the RM effect is greater.

2.3 Planetary rings

Planetary rings are composed of a vast number of tiny particles believed to either have been left over during the formation of the planet or formed as a result of tidal break up

of moons (Miner et al., 2007). All the giant planets in our Solar System have planetary rings with varying sizes, albedo, optical depth and composition. The rings are very thin compared to their radial extents. Saturn having the largest and brightest rings has been subjected to a variety of ring studies in quests to explain the formation, dynamics and composition of its rings (Charnoz et al., 2009; Estrada and Cuzzi, 1996; Hahn and Spitale, 2013). Saturn's rings consist mostly of water ice making it very bright (Nicholson et al., 2008), Uranus and Neptune have thin dark rings separated by large gaps while Jupiter's rings are faint and believed to have formed from impact ejecta from small moons (Lissauer and de Pater, 2013).

2.3.1 Physical constraints on planetary rings

Any satellite around a planet has to be located within a distance from the planet where the gravitational influence of the planet dominates over external forces from the host star. This is referred to as the Hill radius R_H of the planet and it is given for a circular orbit as

$$R_H = a\left(\frac{M_p}{3M_*}\right)^{1/3} = R_p\left(\frac{GP^2\rho_p}{9\pi}\right)^{1/3}, \tag{2.9}$$

where ρ_p is the density of the planet. This implies that the Hill radius is the maximum distance at which a satellite can orbit a planet.

Within a distance referred to as the Roche radius of the planet, a large satellite of density ρ_s will disintegrate due to the tidal forces of the planet exceeding the gravitational self-attraction of the satellite. The Roche radius R_R of a planet with density ρ_p is given as

$$R_R = 2.45R_p\left(\frac{\rho_p}{\rho_s}\right)^{1/3}, \tag{2.10}$$

it depends on the density (thus internal material strength) of the satellite. Rings would be expected to form within the Roche radius from the disintegrated satellite which spread out from the point of break-up. Conversely, any material beyond the

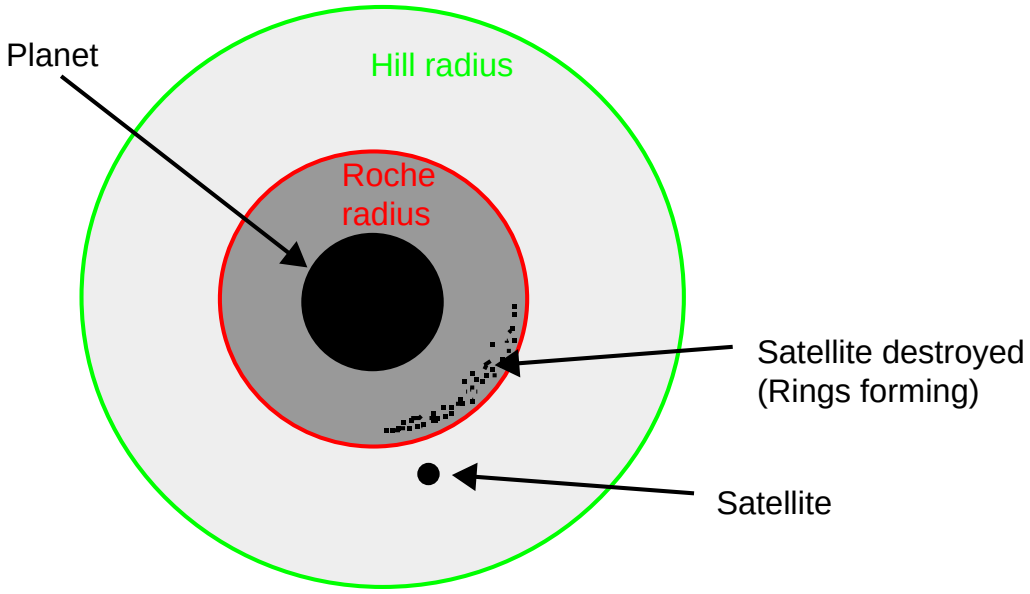

FIGURE 2.3: Schematic representation of the Hill and Roche radii around a planet. Satellites break up to form satellites with Roche radius.

Roche radius but still within the Hill Radius will again coalesce to form large satellites (moons). Illustration of the Hill and Roche radii around a planet is shown in Fig. 2.3. R_H is expected to be larger than R_R for satellites and for stable rings. The main rings of all the Solar System giant planets are within the respective Roche limits of the planets (Miner et al., 2007). An exception to this are the extended G and E rings of Saturn which lie outside the Roche radius thereby rendering the explanation of their formation from satellite break up implausible. The E rings are believed to be formed from materials being ejected from Saturn's moon Enceladus (Miner et al., 2007).

2.3.2 Rings around exoplanets

Rings around exoplanets will have to obey the same dynamical arguments previously mentioned. They have to be within the Hill radius and Roche Radius. The Hill sphere

is however considered to be unstable in its outer regions (Hamilton and Burns, 1991; Neto and Winter, 2001). Therefore, rings can only form when the Roche radius is within the stability region of the Hill sphere so we must have $R_R \ll R_H$ as we have in the Solar System. Close-in exoplanets can have $R_R \sim R_H$ which will preclude formation of rings due to the lack of bound states in outer regions of Hill sphere (Schlichting and Chang, 2011). Therefore, a search for rings around close-in exoplanet should be only for those planets which have $R_R \ll R_H$.

For icy rings similar to that of the main rings of Saturn to exist around a planet, Gaudi et al. (2003) showed that the planet must have a semi-major axis greater than

$$a \simeq \left(\frac{L_*}{16\pi\sigma T_{sub}^4}\right)^{1/2} = 2.7\text{AU}\left(\frac{L_*}{L_\odot}\right)^{1/2}, \tag{2.11}$$

where $T_{sub} = 170\,\text{K}$ is the ice sublimation temperature and L_* is the luminosity of the star. This implies that close-in planets cannot have rings composed of ice. However, Schlichting and Chang (2011) investigated the nature of the rings around close-in planets and proposed the possibility of rock-like rings instead of the icy rings around our Solar System planets. They also emphasized the possibility of detecting these rings at semi-major axes larger than 0.1 AU.

For close-in ringed exoplanets, the action of forces like Poynting Robertson drag and viscous friction from planet exosphere can act to remove ring particles from the system (Goldreich and Tremaine, 1982). These forces cause the ring particles to lose angular momentum and spiral into the planet. Schlichting and Chang (2011) showed that if rings are optically thick, they can have a longer life time of up to 10^9 years based on the action of the Poynting-Robertson drag whose effect supercedes other ring disrupting forces.

Chapter 3

SOAP3.0 and ringed planet transit

3.1 SOAP3.0

SOAP3.0 is a numerical tool developed as a modification to the planet transit tool SOAP2.0-T by Oshagh et al. (2016). SOAP2.0-T is an adaptation of SOAP (Boisse et al., 2012) and SOAP2.0 (Dumusque et al., 2014) in order to simulate the photometric and radial velocity variations of a planet transiting a rotating spotted star. It generates transit light-curve and Rossiter McLauglin (RM) signal due to the transiting planet. Detailed description of these tools can be found in Boisse et al. (2012), Oshagh et al. (2013), and Dumusque et al. (2014).

SOAP3.0 is developed to simulate the transit light-curve, RM signal and the induced anomalies in these signals due to the transit of the ringed planet. This tool is also capable of generating the signal variations due to occultation of stellar active regions by the ringed planet but this functionality is not used here as it is not the the focus of this thesis.

To add the effect of rings to the computation, I assumed that rings are circular, geometrically thin and completely opaque. The rings lie beyond the planet's radius and blocks stellar light in the same way as the planet but only between inner and outer radii defined by R_{in} and R_{out}. The ring orientation is defined by two angles: i_r, the inclination of the ring plane with respect to the sky plane (0^o and 90^o for face-on and edge-on projections respectively) and θ, the tilt of the ring plane to the planet's orbital plane (0^o and 90^o for ring projection parallel and perpendicular to orbital plane

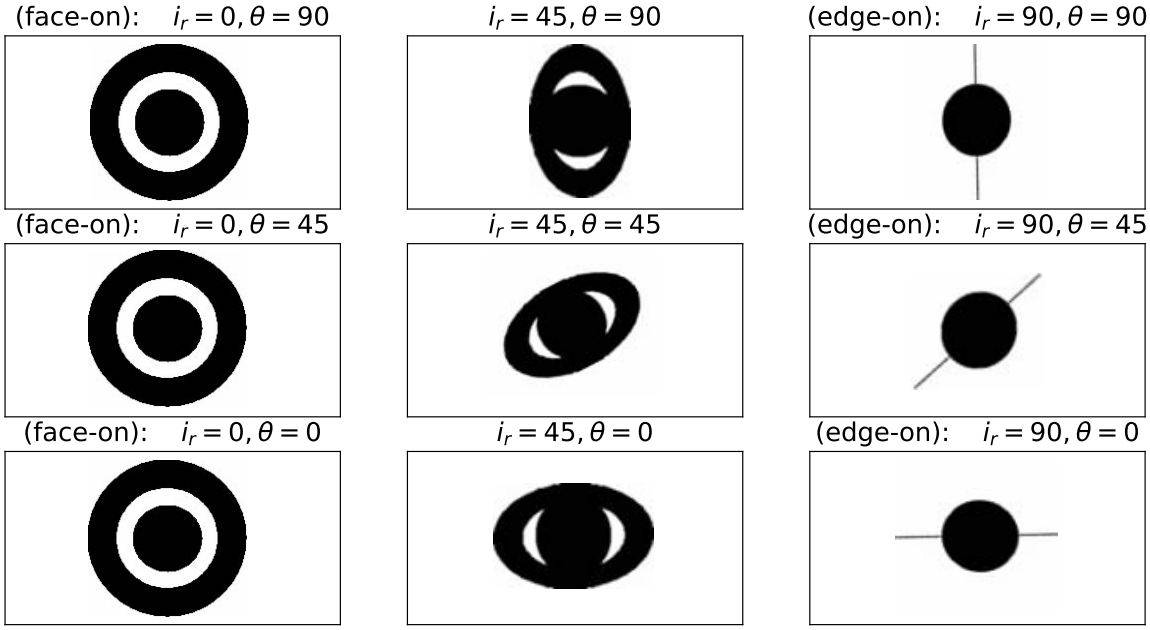

FIGURE 3.1: Illustration of a planet with 9 different ring orientations defined by i_r and θ.

respectively). Fig. 3.1 illustrates different ring orientations for a planet. It is assumed that the ring maintains the same orientation throughout the transit phase[1].

For the computation, a square grid of $N \times N$ cells is defined to cover the entire stellar disk. The flux and RV contribution from each cell is calculated during the transit of planet+ring.

3.1.1 Input parameters

SOAP3.0, as with the predecessor tools, is supplied with input parameters through a configuration file "config.cfg". Inputs are as defined in Oshagh et al. (2013). The description of the relevant input parameters for ringed planet transit is provided below.

For a spherical ringless planet transit, the input parameters are: the radius of the planet R_p (in units of stellar radii R_*), the semi-major axis a (in units of stellar radii), planet orbital inclination i_p, and the planet's orbital period P (in days) calculated from a and stellar mass using Kepler's third law (eqn. 2.4). The impact parameter b can

[1]Transit duration is much shorter than the orbital period, which is the case for most exoplanets, so change in ring orientation during transit is negligible.

TABLE 3.1: Simulation Parameters selected to satisfy the ring constraints in 2.3.2

Parameter	Value	Description
R_* [$R_\odot$]	1.0	Stellar radius
u_1, u_2	0.29, 0.34	Limb darkening coefficients
$\nu \sin i_*$ [km/s]	2	Stellar rotation velocity
a [R_*]	36.08	Semi-major axis
P [days]	25	Orbital period
i_p [°]	90 ($b = 0$)	Orbital inclination
R_p [R_*]	0.1	Planetary radius
λ [°]	0	Spin-orbit misalignment angle
R_{in} [R_p]	1.5	Ring inner radius
R_{out} [R_p]	2.0	Ring outer radius
i_r [°]	[0,90]	Ring inclination
θ [°]	[0,90]	Ring tilt

be calculated using $b = a \cos i_p$. Additional inputs include: periastron passage time t_0, eccentricity e, argument of periastron ω and the planet's initial phase ψ_0.

For the ring, the input parameters to the code are: inner ring radius R_{in} and outer ring radius R_{out} both in units of planet radii (R_p). Also the two orientation angles: inclination i_r and tilt θ both in degrees.

3.1.2 Outputs

The output of the code gives the Flux, RV, BIS (bisector span), and FWHM[2] variations and can be plotted as a function of stellar rotation phase, orbital phase or time. Details of how these variations are computed can be seen in Boisse et al. (2012), Oshagh et al. (2013), and Dumusque et al. (2014).

3.1.3 SOAP3.0 transit signals: Light-curve and RM signal

To illustrate the output of SOAP3.0, simulation of the transit of a short-period planet is done with ∼200 s (3.5 mins) time-sampling using fiducial values in Table 3.1. The planet is a Jovian-like planet with a semi-major axis of 0.16 AU (36.08 R_*) assumed to follow a circular orbit around a Solar-like star with $T_{\rm eff}$=5778 K. The stellar rotation

[2]Full Width at Half Maximum of cross correlation function

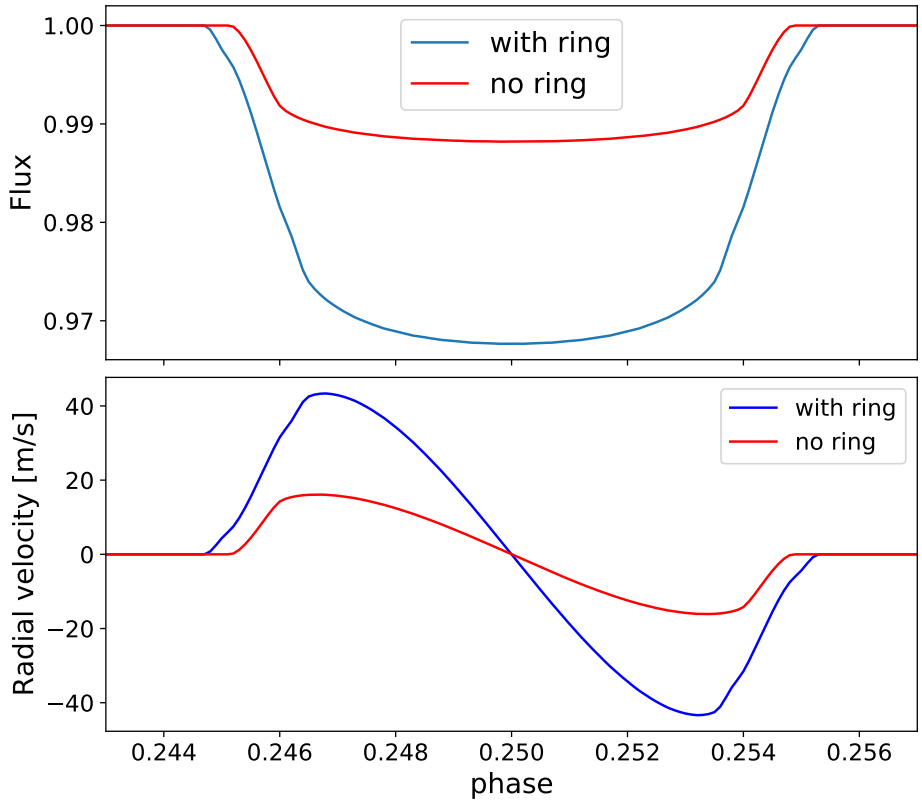

FIGURE 3.2: SOAP3.0 Light-curve (top) and RM signal (bottom) as a function of orbital phase for a transiting planet without a ring (red) and with a ring (blue) at face-on orientation $(i_r, \theta = 0, 0)$. The ringed planet produces a longer transit of 6.38 hrs compared to 5.85 hrs for the ringless planet.

axis is assumed to be parallel to the sky plane XY. Stellar quadratic limb darkening coefficients given by Claret and Bloemen (2011) are used for the star described.

Fig. 3.2 shows the transit light-curve and RM signal for a spherical ringless planet and for the same planet having the ring parameters in Table 3.1. The ring orientation is face-on (i.e. $i_r = 0$). It is seen that the ringed planet produces a deeper photometric transit and greater RM amplitude than the ringless planet. This is due to the additional stellar disk area covered by the ring. Also since the ring increases the projected radial extent of the planet, it causes a longer transit duration (6.38 hrs). This light-curve and RM signal can however be easily produced by a planet with a larger radius.

A feature more indicative of the presence of ring is the anomaly seen when the ring's outer edge, inner edge and planet edge contact the stellar disk at ingress/egress phases. These anomalies manifest as wiggles in the transit light-curve and RM signal

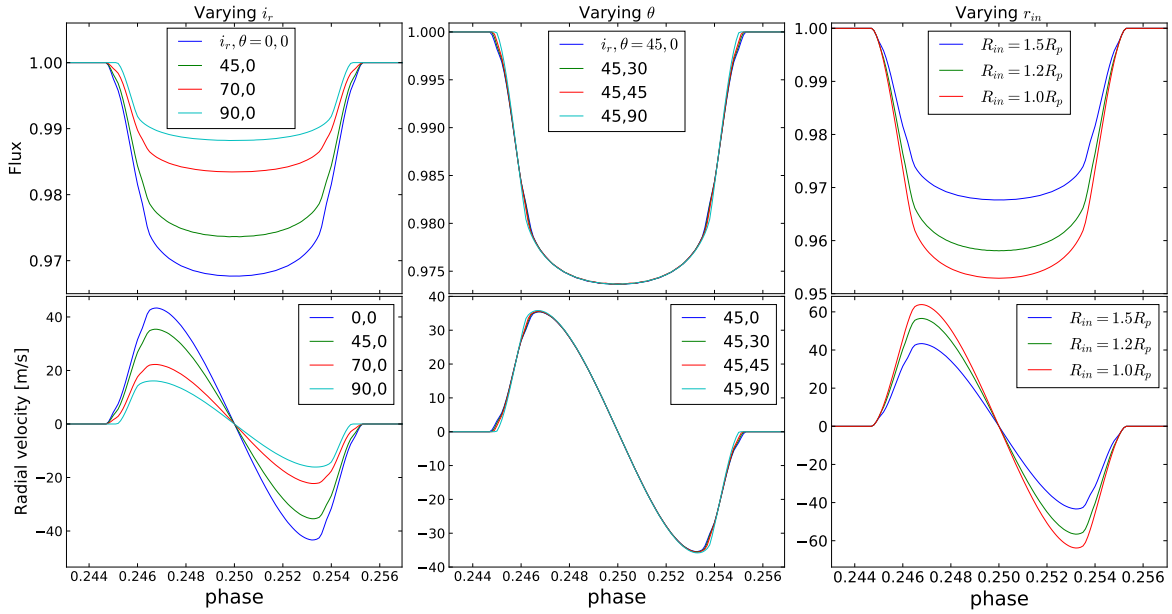

FIGURE 3.3: Effect of varying ring parameters on the light-curve and RM signals. First column shows the how the light curve and RM signal varies for different values of i_r. Second column shows signal variation for different values of θ when $i_r = 45$. Third column shows the effect of varying the gap between planet surface and ring area by varying R_{in}.

during ingress and egress as seen in Fig. 3.2. Therefore, the detection/identification of exoplanetary rings depend on the ability to detect and measure these wiggles as will be seen in Chapter 4.

For the same planet, the transit signals vary as the parameters of the ring changes. Fig. 3.3 illustrates the effect of ring parameter changes on transit light-curve and RM signal. As seen in its first column, varying i_r from face-on ($i_r = 0^o$) up to edge-on ($i_r = 90^o$) causes the transit signals to decrease in amplitude due to the reduction in ring projected area with i_r. At edge on, the light-curve and RM signal of the ringed planet appears indistinguishable from that of the ringless planet since the thickness of ring is negligible and does not block any stellar flux. The second column shows the signals when i_r is kept at 45^o and θ is varied from 0^o to 90^o. It is seen that the signals do not vary very much with θ, its most visible effect is to slightly reduce the transit duration as it approaches 90^o. The third column of Fig. 3.3 shows the effect of changing the inner radius of the ring while the outer radius remains at the constant value in Table 3.1. The value of R_{in} determines the size of the gap between

planet surface and ring and it is seen that as the gap size reduces the signal amplitude increases due to increasing ring area.

The plots in Fig. 3.3 has shown that varying ring parameters mostly affects the amplitude and to a much lesser extent the duration of the transit signals. More subtle variations can be noticed in the prominence of the wiggles at ingress/egress as the ring parameters change. The variation in the prominence of the wiggles with ring parameters can be used to detect and characterise the signature of the ring.

3.2 Performance test of SOAP3.0

SOAP3.0 is capable of producing precise transit light-curves and RM signals for spherical planet transit as shown by Oshagh et al. (2013). For this thesis, it was important to debug, test and validate that our inclusion of rings provide the expected output.

After the necessary tests and modifications were performed to ensure proper computation, the ringed planet photometric results of SOAP3.0 was compared with those from *EXORINGS* (Zuluaga et al., 2015) and Tusnski and Valio (2011). Table 3.1 was used to generate mock transits of a ringed planet with both SOAP3.0 and *EXORINGS* and their results were compared. Also, comparison with transit result shown in Tusnski and Valio (2011) was done using same input parameters as the paper. The results of these comparisons are summarised in Table 3.2 and Fig. 3.4. *EXORINGS* does not consider limb darkening whereas SOAP3.0 uses a quadratic limb darkening law (more realistic case) causing their results to be different. However, when limb darkening was also ignored in SOAP3.0, both tools show excellent agreement. For some orientations, especially at edge-on (i_r=90°) where the ring should have no contribution to transit duration and depth (since they are assumed to be infinitely thin), *EXORINGS* calculates the transit duration incorrectly.

Comparison with Tusnski and Valio (2011) (TV11 in table 3.2) shows similar results for transit duration but not with transit depth. This is because SOAP3.0 assumes completely opaque rings while Tusnski and Valio (2011) model uses opacity τ=0.5

TABLE 3.2: Comparison of SOAP3.0 with *EXORINGS* using Table 3.1 input. Also comparison with quoted values of Tusnski and Valio (2011) using input values from the paper. SOAP3.0(LD) corresponds to results when limb darkening is used. Asterisk (*) denotes orientations where the transit duration of *EXORINGS* and SOAP3.0 differs.

Ring angles		Transit depth (ppm)			Transit duration (hours)	
i_r	θ	*EXORINGS*	SOAP3.0	SOAP3.0(LD)	EXORINGS	SOAP3.0
0	0	27500	27515	32387	6.380	6.383
20	0	26444	26450	31144	6.380	6.383
45	0	22374	22387	26364	6.380	6.383
70	0	14047	14052	16567	6.380	6.383
*90	0	10000	10000	11792	6.380	5.850
*0	45	27500	27515	32387	6.026	6.383
*90	45	10000	10000	11844	6.024	6.350
[*TV11*] input:$R_p = 0.084R_*$, $R_{in} = 1.11$, R_{out}=2.32, i_p=88°, $\tau = 0.5$, (u_1, u_2)=(0.2925,0.3475)						
i_r	θ	TV11	SOAP3.0	SOAP3.0(LD)	TV11	SOAP3.0
78	20	10500	10800	12374	3.40	3.41

($\tau = [0, 1]$). However, it is noted that since the opacity and ring area are degenerate parameters, one can compensate for the opacity by reducing the area of the ring. For instance, a ring with $\tau = 0.5$ can be mimicked by an opaque ring with half the area. Indeed when this is done, the transit depth obtained is similar to Tusnski and Valio (2011). It is emphasized here that this comparison was done based on visual inspection of the light-curve in the paper since there was no access to the code used.

Comparison of SOAP3.0 ringed planet RM signal with that of Ohta et al. (2009) was not done due to difference in RV measurement technique employed in the models (Boué et al., 2013). Ohta et al. (2009) computes weighted mean velocity along stellar line of sight whereas SOAP3.0 performs a gaussian fit to a cross-correlation function (Boisse et al., 2012) as is done on stabilized spectrographs. Inspite of this, visual comparison of the paper result with that of SOAP3.0 shows that the shape of the RM signal and wiggles are very identical. It should be noted that a ringed planet RM signal would be different from that of a spherical planet irrespective of the RV measurement technique used as long as one is consistent with the technique used in both ringed and

ringless cases.

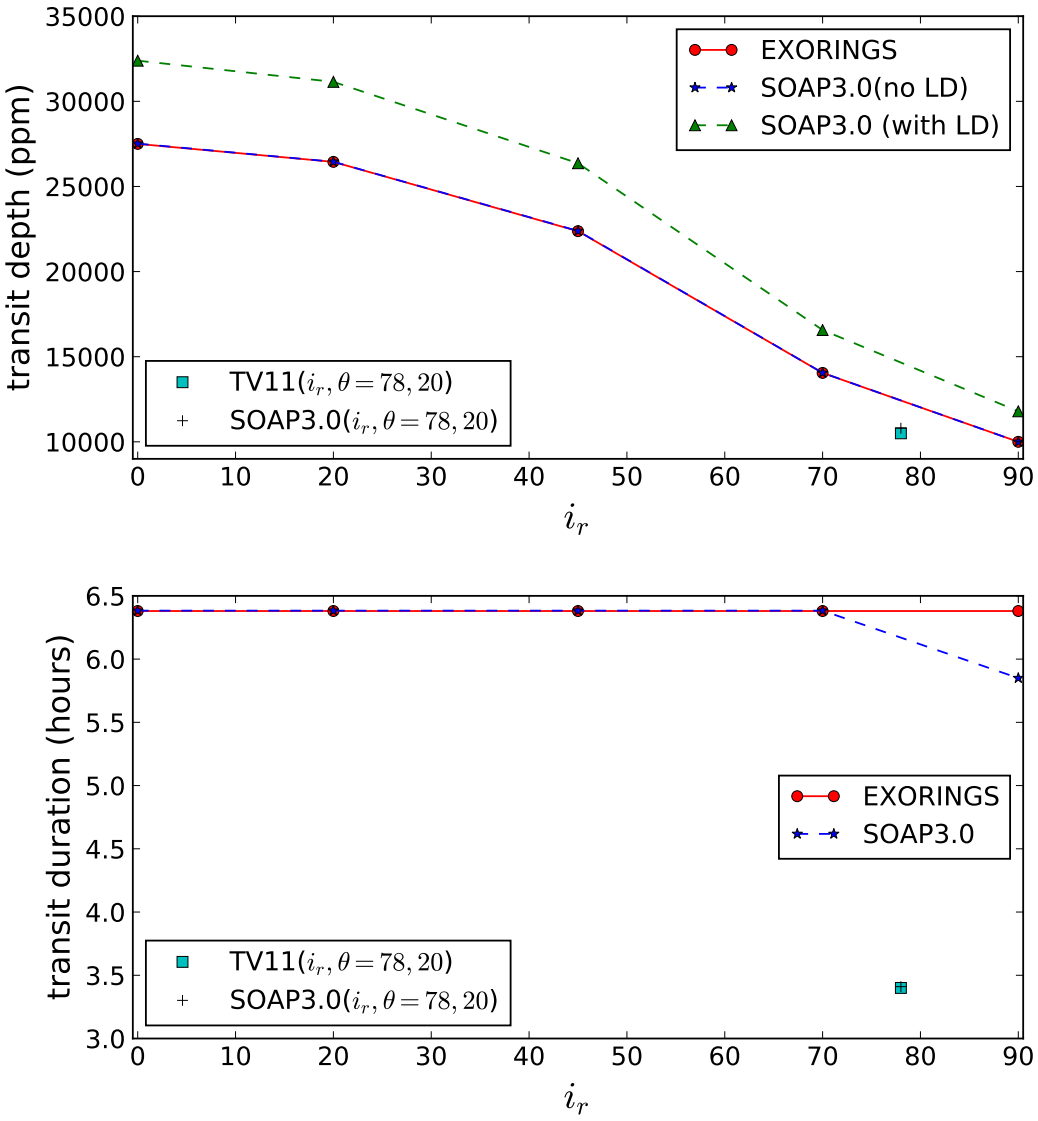

FIGURE 3.4: Comparisons of SOAP3.0 results with those from EXORINGS and Tusnski and Valio (2011) [TV11]. Transit depth (left pane) and transit duration (right pane) as a function of i_r for $\theta = 0$ computed using *SOAP3.0* and *EXORINGS*. Also comparison of SOAP3.0 with TV11 for $i_r, \theta = 78, 20$. Green triangles are points from SOAP3.0 using solar limb darkening, blue asterisks are points from SOAP3.0 without limb darkening and the red circles are points from *EXORINGS*. Cyan squares and black crosses are the points from TV11 and SOAP3.0 respectively for $i_r, \theta = 78, 20$.

Chapter 4

Detecting ring signatures

It is imperative to be able to discern the signature of potential rings in light-curves and RM signals. Therefore, this chapter describes the method employed in detecting ring signatures. The ring signature in a transit signal would be the residual between the ringed planet signal and the best-fit ringless planet model (Barnes and Fortney, 2004). The maximum residuals indicating the ring signature should therefore be positioned around ingress and egress.

4.1 Ringed planet simulation and ringless fit

A combination of 9 different ring inclinations (i_r) and 7 different ring tilt angles (θ) were simulated to cover the range of all possible ring orientations. Therefore a total of 63 ringed planet transits having different i_r, θ combinations were simulated with SOAP3.0 using fiducial values in Table 3.1.

Using theoretical model of Mandel and Agol (2002), the simulated ringed planet transit light-curves were fitted with a ringless planet model. R_p, a and i_p were allowed to vary as free parameters while the limb darkening coefficients (LDCs) u_1 and u_2 were fixed by assuming they are known a priori (e.g. from Claret and Bloemen 2011 or Sing 2010). The impact of not fixing the LDCs will be probed in chapter 5. For each light-curve fit, the residuals were computed and the maximum absolute residual (which should be at ingress/ingress) was calculated.

Using the numerical tool SOAP2.0-T which does not account for the ring, fitting of the 63 simulated ringed planet RM signals was performed with a ringless planet model.[1] Initially, the fitting was done with $\nu \sin i_*$, λ, R_p and i_p as free parameters while the other parameters were fixed to values in Table 3.1. This was done to investigate whether the presence of rings around an exoplanet could make a planet seem misaligned or cause an inaccurate estimation of $\nu \sin i_*$. The values of $\nu \sin i_*$ and λ were found not to change and because performing a numerical fit is computationally intensive, the free parameters were reduced to R_p and i_p. The residuals of each RM signal fit were obtained and the maximum absolute residual calculated.

Fig. 4.1 shows the fits to the light-curves and RM signals of the simulated face-on and edge-on ringed planet transits. The plots also show the residuals with maximum amplitudes at ingress and egress. As expected, the edge-on ringed planet signals show no ring signature in the residuals. On the other hand, fits to the light-curve and RM signal of the face-on ring planet produces large residuals (3.15 m/s for RM and 455 ppm for flux) at ingress/egress with a duration of 70 mins. The light-curve residual plot shows symmetry about mid transit phase (0.25) while the RM residual plot shows anti-symmetry. In order to accurately detect the ring signature, a photometric noise level $\leq$100 ppm and RV precision of 1 m/s is required for each exposure. Therefore, we set 100 ppm and 1 m/s as the photometric and RV detection limits. These are reasonable limits based on the precisions of current and near-future instruments. These limits are shown as dashed lines in the residual plots. The impact of these limits is explored in Chapter 5.

As seen in Fig. 4.1, the R_p derived from the face-on ringed planet fit is greater than the actual planet radius used in Table 3.1. This greater radius would lead to an underestimation of planetary density if planet mass were known. Perhaps the large

[1] Other analytical tools such as ARoME (Boué et al., 2013) could have been used for fitting the RM signals. However, this was not used because we are concerned only with the impact of the rings and do not want to be affected by the slight difference between the RM signals from ARoME and SOAP3.0. This difference arises from approximations used in the analytical tool (Boué et al., 2013; Oshagh et al., 2016).

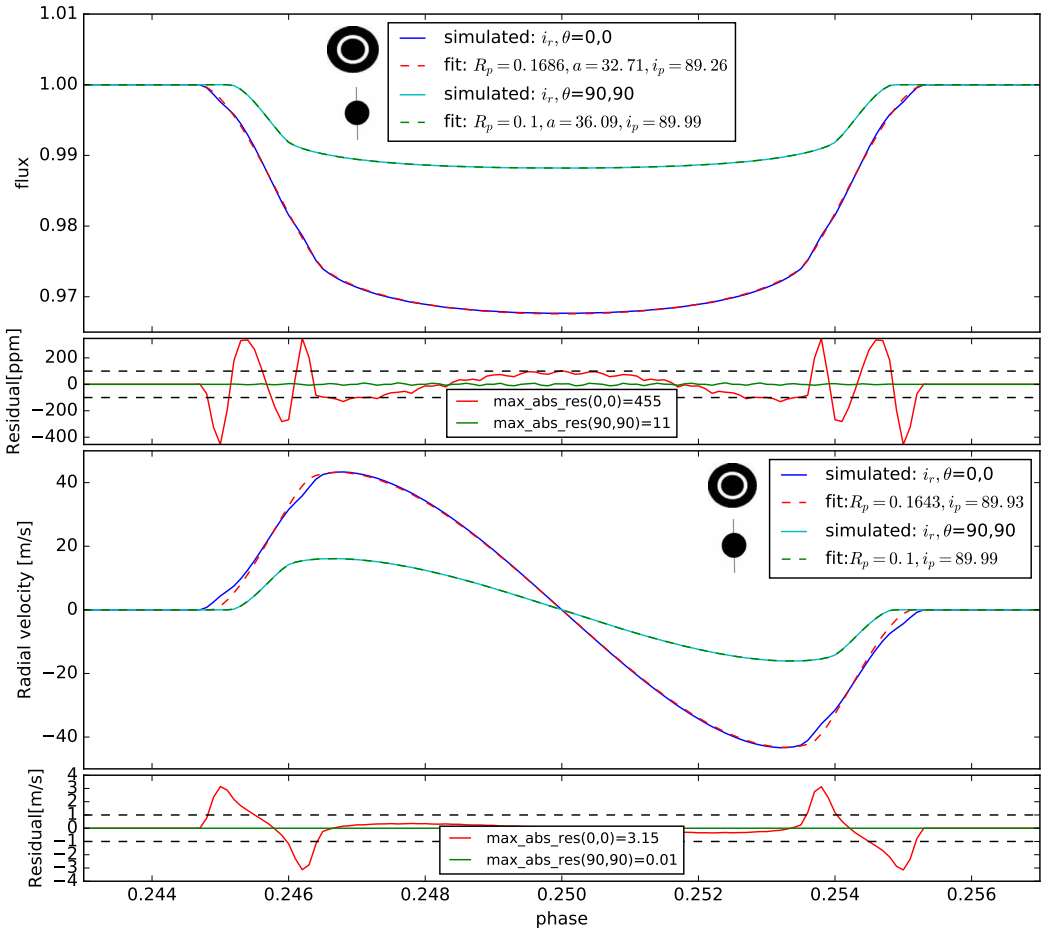

FIGURE 4.1: Ringless model fit to two ring orientations (face-on and edge-on) of the ringed planet. Left pane shows the analytical ringless fit to the two ringed planets light-curves and the respective residuals generated. Right pane shows the numerical ringless fit to the two ringed planet RM signals and the residuals. The black dashed line in residual plots show the detection limit as mentioned in text.

radii and low densities of highly inflated hot Jupiters (Anderson et al., 2010; Hartman et al., 2012) can be explained by the presence of rings if it is at all possible for the rings to form at these short distances ($a < 0.1$ AU) from the star.

As shown in Zuluaga et al. (2015) for the photometric transit, the a and i_p derived for most orientations of the ring will be underestimated (compare light-curve fit values in Fig. 4.1 to values in Table 3.1). In-turn, the transit-derived stellar density (eqn. 2.5) would be underestimated when compared to asteroseismology derived stellar density (Santos et al., 2015). Perhaps, the discrepancies between both methods for derivation of stellar density (Huber et al., 2013) could be explained by the presence of planetary

rings amongst other explanations (Kipping, 2014).

The light-curve residuals of the edge-on ring produces some high-frequency irregularities around mid-transit phases with maximum absolute residual of 11 ppm. This is due to numerical noise in SOAP3.0 light-curve computation (see also Fig. 3 of Oshagh et al. 2013) but these irregularities are far below the detection limit considered. These mid-transit irregularities from the code are also present for the face-on ring and an additional non-linear trend is noticed in this region. This trend arises from the non-linear limb darkening law whose coefficients cannot compensate for the different inclination (i_p) derived from the fit (Barnes and Fortney, 2004). But since ring signatures are localized to ingress/egress phases, the trend around mid-transit phases (which is smaller than detection limit) do not interfere with the accuracy in measuring the ring signatures.

4.2 Identifying favorable ring orientations for detection

It is important to identify the possible ring orientations that will favour detection. To do this, the light-curve and RM fit for all 63 ring orientations was performed taking note of the maximum absolute residual (ring signature) in each case.

Fig. 4.2 shows contour plots generated using the maximum absolute residuals of each ring orientation with the overplotted asterisks indicating the orientations from which the residuals were obtained. It is seen for the light-curve and RM residuals that several of the ring orientations favor easy detection using the detection limits we set.

For all θ values within $i_r \leq 30^{\circ}$ (at and around face-on), the ring signatures are very prominent both for the light-curve and RM signal due to large stellar area covered by the ring. However, as i_r increases up to 70° for the RM and 80° for light-curve, good detectability gradually shifts to only values of $\theta \leq 30^{\circ}$. A blue band of low or

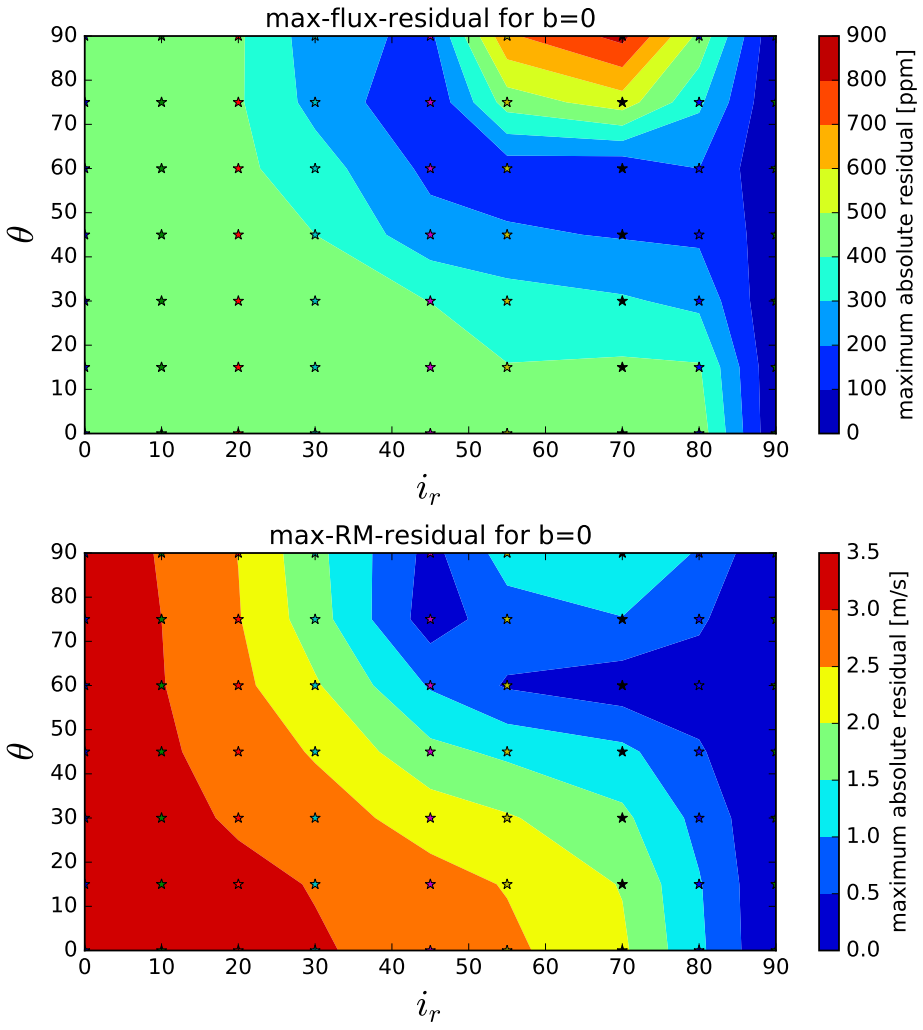

FIGURE 4.2: Contour plot from maximum absolute residual obtained from fit of 63 ring orientations. Top plot shows the contour plot for the light-curve fit while bottom plot shows the contour plot for the RM fit.

undetectable ring signature for light-curve and RM signal is noticed for points inside about $i_r > 40^o$ and $\theta > 40^o$ up to all edge-on ($i_r \simeq 90^o$) orientations. This indicates that transit signal with ring orientation within this blue region can nearly be approximated by a ringless transit model.

A separate region with high ring signature is evident in the residual of the light-curve fit centered around $i_r, \theta = 70^o, 90^o$. Around this orientation, the high i_r causes only a small projected ring area whereas $\theta = 90^o$ makes the ring perpendicular to the orbital plane. This causes the transit duration to be the same as that of a ringless

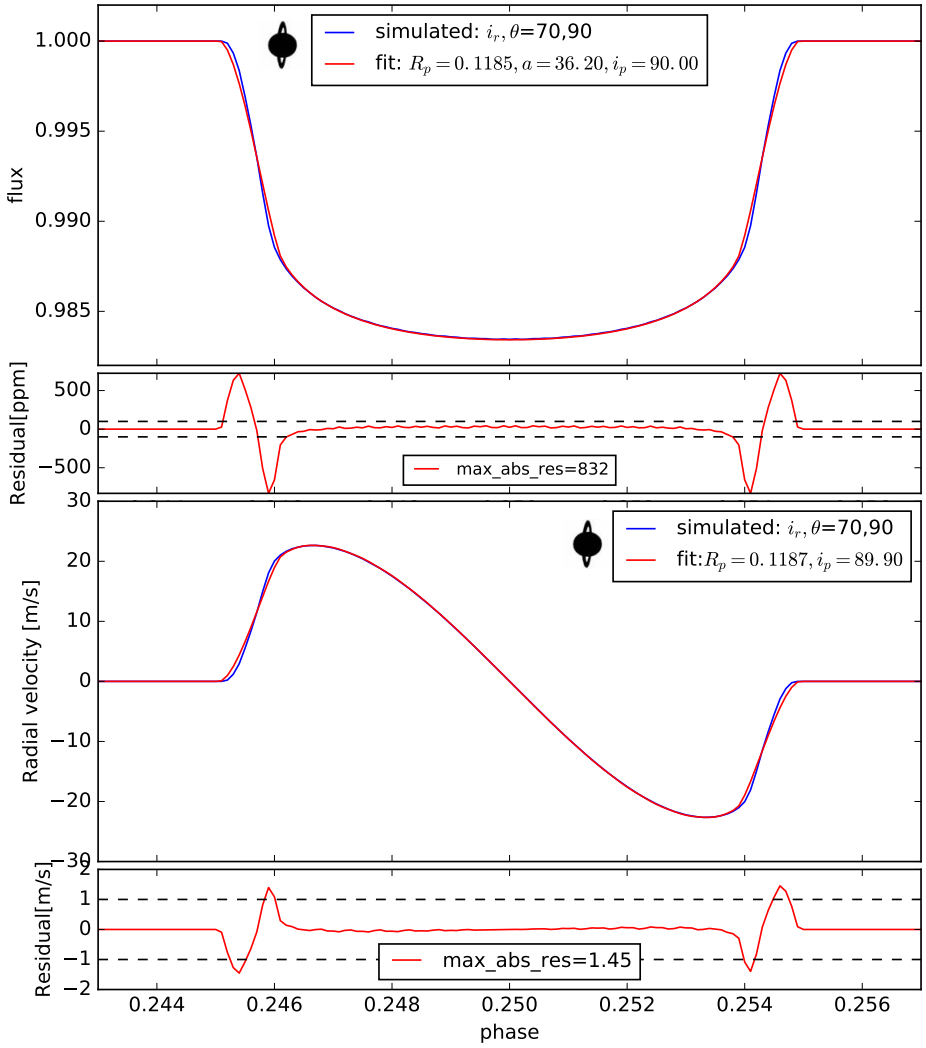

FIGURE 4.3: Light curve and RM signal fit for $i_r, \theta = 70^o, 90^o$.

planet but there would be an increased transit depth. A ringless fit is unable to perfectly reconcile the transit duration with the depth thereby causing an overestimation of the duration which leads to a high residual at ingress/egress. This is also observed for the RM residual in this region although not nearly as significant as that of the light-curve. The plot of this orientation is shown in Fig. 4.3.

It is therefore seen that a lot of the ring orientations favor detection although most of them are close to face-on where a greater stellar area is covered by the ring. However, for close-in ringed planets, the inclination i_r is expected to have been damped towards edge-on due to tidal forces from the star making ring detection difficult (Schlichting

and Chang, 2011; Heising et al., 2015). Schlichting and Chang (2011) also showed that exoplanets with $a > 0.1$ AU can have i_r values that favor detection. If we take $i_r \geq 45^{\rm o}$ to represent feasible exoplanetary ring inclinations for this close-in planet then we have quite a number of orientations in Fig. 4.2 with high ring signatures interesting for the search for exoplanetary rings. We will explore how the ring signatures change with impact parameter in Chapter 5.

Chapter 5

Discussion

In this section we discuss the impact of some assumptions and other effects that may come into play in the detection of exoplanetary rings.

5.1 Effect of ring-planet gap and ring area

As seen in the third column of Fig. 3.3, the gap between ring and the planet's surface and also the variation of the ring area changes the ringed planet's signal. We assess here how these changes impact the ring signature. To assess the gap impact, the face-on ring orientation is again selected with the value of R_{in} varied from $1\,R_p$ up to $1.5\,R_p$ while maintaining a constant ring area. The amplitude of ring signature is extracted from the fit. The left column of Fig. 5.1 shows that as the planet-ring gap increases, the ring signature also increases both for the flux and RM. When ring is in contact with planet surface at face-on, the ringed planet signal is the same as that of a ringless planet with a larger radius since the ring here is optically thick. However, if the ring is only nearly face-on, the transit light-curve would be identical to that of a very oblate planet (Barnes and Fortney, 2003).

The impact of ring area is assessed by keeping $R_{in} = 1.5\,R_p$ while increasing the value of R_{out} from $2\,R_p$ up to $3R_p$. The right column of Fig. 5.1 shows that the ring signature also increases with ring area in the flux and RM. As ring area increases, the transit signal of the ringed planet gets increasingly similar to the grazing eclipse of a binary star having a V-shaped light-curve.

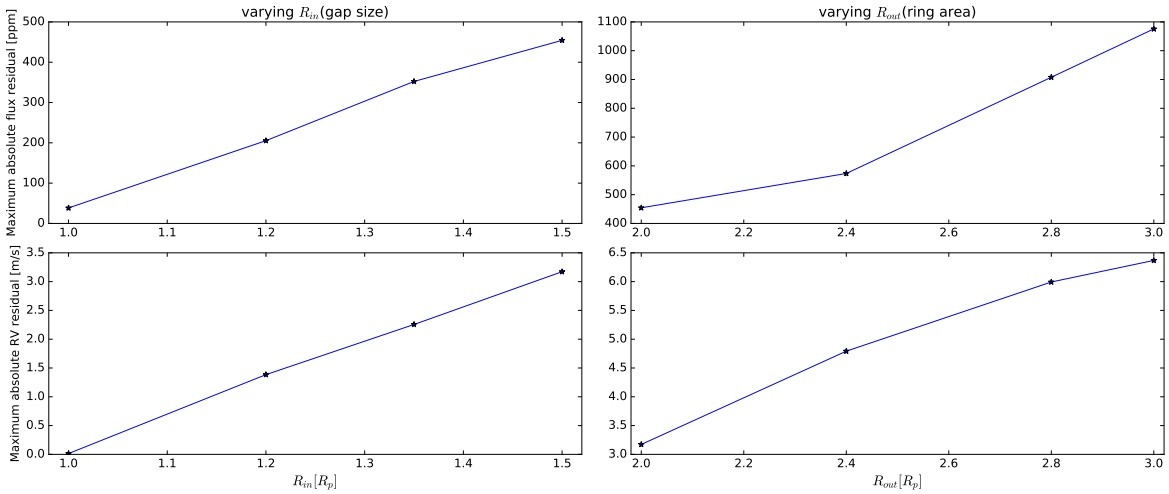

FIGURE 5.1: Left column: Effect of planet-ring gap on ring signature by increasing R_{in}. Right column: Effect of ring area on ring signature by increasing R_{out}. Top plots are the effects in flux and bottom plots are the effects in RV

Thus the finding suggests that it is easier to detect rings with larger planet-ring gap and larger ring area.

5.2 Effect of limb darkening

For most fitting procedures, if the limb darkening coefficients (LDCs) are known a priori they are fixed during the fitting as was done in Chapter 4. This reduces the amount of free parameters thereby increasing accuracy of the results and could eliminate some degeneracy in the fitting process. However, limb darkening affects transit signals at ingress, egress and signal amplitude and so can compete with ring signature. The impact of inaccurate estimation of LDCs (u_1,u_2) on the detection of the ring signature both in the light-curve and RM signal can be assessed by fitting them as free parameters. The face-on ring orientation is used for this test and the result is shown in Fig. 5.2.

It is seen that fitting the LDCs give rise to an inaccurate estimation of the LDCs. Comparing the free-LDC fit residual to the fixed-LDC fit residual shows that the inaccurate estimation leads to damping of the ring signature at ingress and egress. For

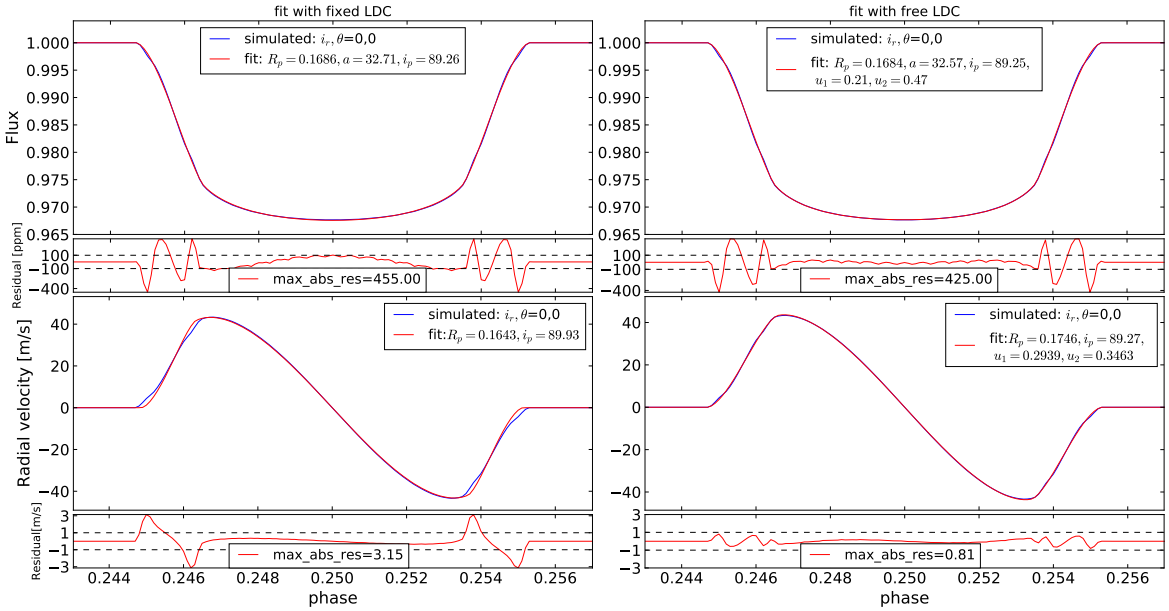

FIGURE 5.2: Effect of fitting ringed planet signal with constant LDC and free LDC. Left column: Fit of face-on ring with LDC kept constant at u_1=0.29, u_2=0.34 for light-curve and RM signal fit. Right column: Fit with LDC allowed to vary.

the light-curve fit, the estimated LDCs are different from the values used for the simulated ringed planet but the residual ring signature is damped only by a small amount. For the RM signal fit, the estimated LDCs are close to that of the ringed planet yet there is a significant damping of the ring signature below the detectable limit of $1\,m/s$. Therefore, inaccurately estimating limb darkening parameters has greater effect in RV and can render ring signatures undetectable.

It has been shown that fitting LDCs in transit analysis can lead to LDCs different from the theoretical LDCs calculated from stellar evolution models (see Barros et al. 2012; Neilson et al. 2017). Therefore, for very high precision transits a very careful modeling of the LDCs needs to be performed so that they don't bias the results (Csizmadia, Sz. et al., 2013).

5.3 Effect of stellar rotation velocity

As shown in equation 2.8, the RM effect is proportional to the projected stellar rotational velocity $\nu \sin i_*$. It is necessary to assess how $\nu \sin i_*$ affects the RM ring

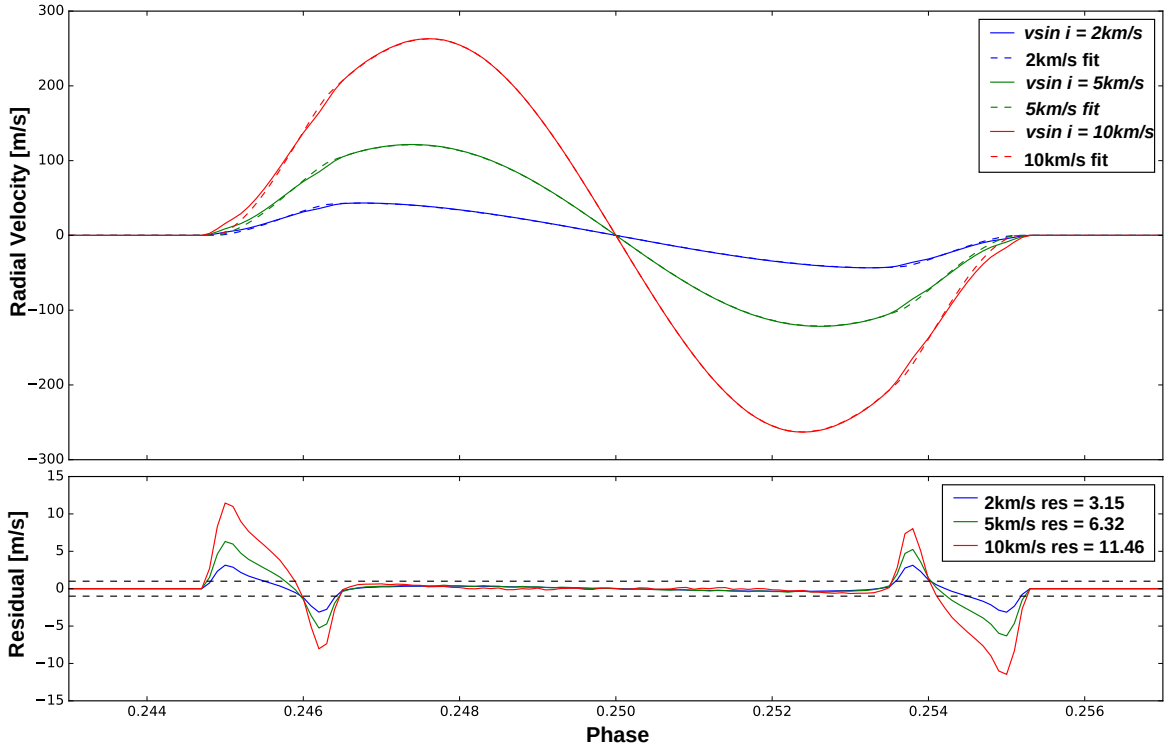

FIGURE 5.3: RM signal for different stellar rotation velocity fitted with a ringless model and their computed residuals in m/s

signature. Using the face-on ring orientation with stellar rotations of 2, 5 and 10 km/s, fits to the generated ringed planet signals was performed and the residuals computed. Fig. 5.3 shows that not only does the RM signal increase with $\nu \sin i_*$ but so does the ring signature. Therefore, it can be easier to detect rings around planets transiting fast rotating stars. However, a fast stellar rotation velocity causes broadening of spectral lines which will degrade the RV precision so a compromise has to be made between stellar rotation velocity and needed RV precision.

5.4 Effect of orbital inclination (impact parameter)

The results in Chapter 4 were obtained for a planet with orbital inclination i_p=90° translating to impact parameter b=0. Here we investigate the ring signatures at impact parameter of 0.7 (i_p=88.89°) by making same contour plot for b=0.7 as was done for b=0 in Fig. 4.2. The contour plot for b=0.7 is shown in Fig. 5.4. It is seen that ring signatures are high even so close to edge-on at i_r = 80° for flux and i_r = 70° for

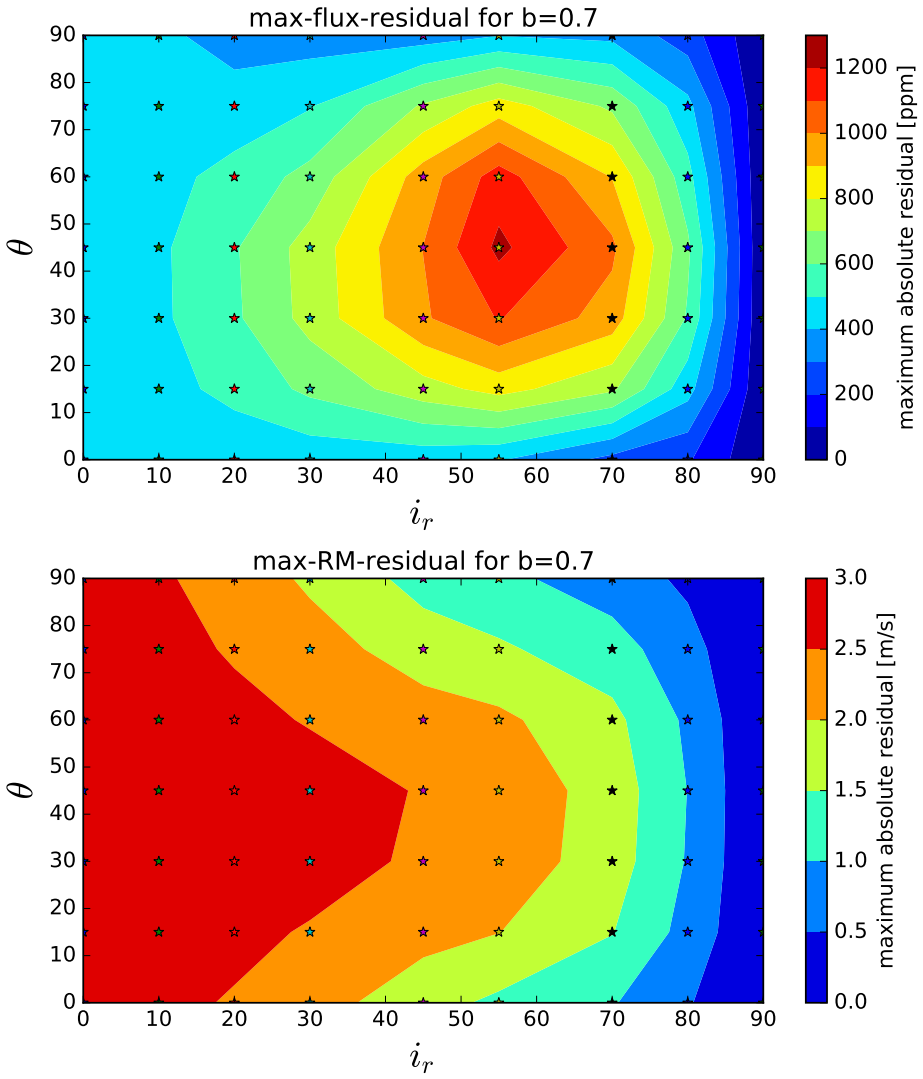

FIGURE 5.4: Contour plot from maximum absolute residual gotten from fit of 63 ring orientations at $b = 0.7$. Top plot shows the contour plot for the light-curve fit while bottom plot shows the contour plot for the RV fit

RM. It is seen in the flux residual from light-curve fit that ring signature is highest at $i_r, \theta = 55^o, 45^o$ and reduces radially from that orientation but goes to zero at edge-on orientations. The high residual at $i_r, \theta = 55^o, 45^o$ is due to asymmetry in the light-curve caused by the ring tilt, high impact parameter, and stellar limb darkening. The light curve is asymmetric because the upper (leading) part of the ring blocks brighter stellar regions during ingress while the lower (trailing) part of the ring blocks a relatively darker region as the ringed planet exits the stellar disc (illustrated in Fig. 5.5). This asymmetry is responsible for high residuals around points where $\theta \neq 0^o$ or 90^o.

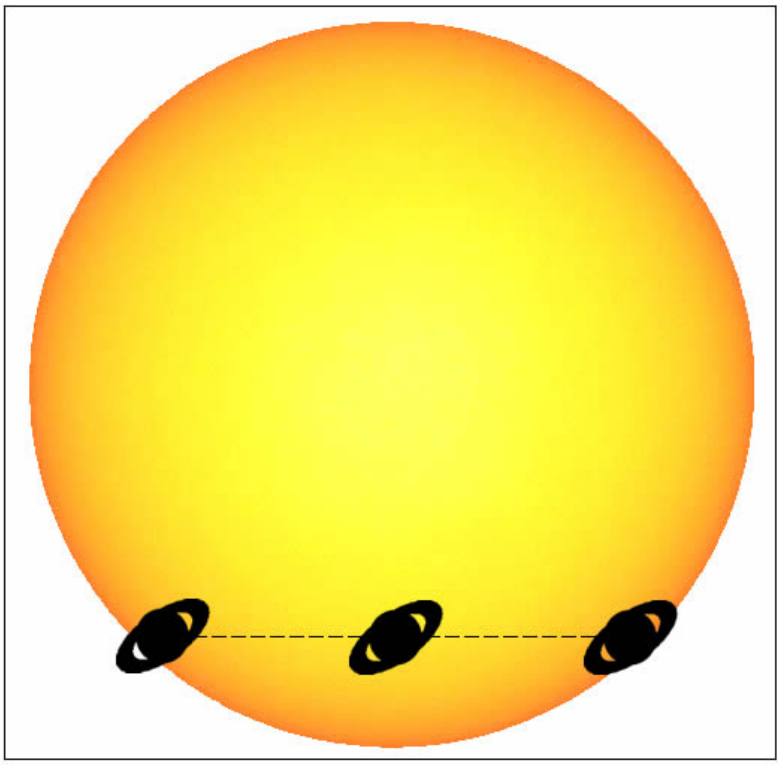

FIGURE 5.5: Illustration of high impact parameter ($b = 0.7$) transit of a planet with tilted ring

The residual from RM signal is highest at and around face-on orientations and reduces gradually to zero towards edge-on orientations. There is also asymmetry in the RM signal for the same reason as above (different parts of the ring blocking stellar regions with different intensities and RV components). The asymmetry is prominent especially around $\theta = 45^{\circ}$ causing a higher residual at $30^{\circ} \leq \theta \leq 60^{\circ}$ than other θ at same i_r. The light-curve and RM signal for the $i_r, \theta = 55^{\circ}, 45^{\circ}$ orientation is plotted in Fig. 5.6.

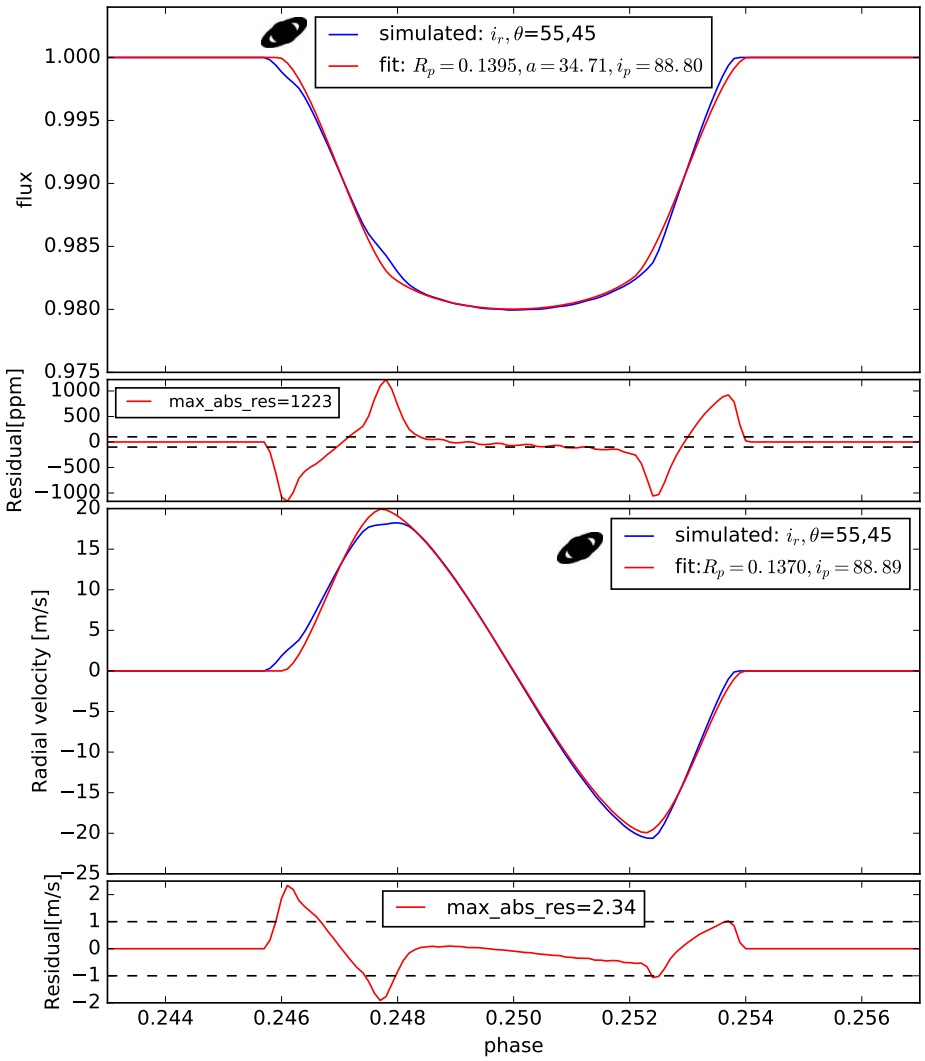

FIGURE 5.6: Asymmetric Light-curve and RM signal of $i_r, \theta = 55, 45$, the ringless fit and residual

5.5 Impact of time-sampling and instrument precision

For the fiducial planet (Table 3.1) on 25-day orbit (0.16 AU), the maximum transit duration (with face-on ring) is 6.38 hrs and the duration of the ring signature at ingress/egress is $\sim$70 mins. The detection of the ring signature in this timescale will require a high precision and high time resolution.

Here we assess the impact of time-sampling and instrument precision on ring signature detection. For long time-sampling, the ring signature might not be well-captured (under-sampled) with the few observational data points whereas for short time-sampling, the noise level per point might be too high to detect the ring signature. Therefore, a compromise has to be reached between the time-sampling and the achieved photon noise limited precision especially in the photometry. Using the fiducial planet with face-on ring, transit signals were simulated with different time-sampling from 30 mins long-cadence to 1 min short-cadence (30, 15, 7, 3.5 and 1 min). The fitting procedure done in Chapter 4 was performed again on each of these transit signals and the residuals are generated. Fig. 5.7 shows the maximum absolute residual gotten for the different time-sampled signals. For each of the time-sampled signals, the precision attained for each exposure should be at/below the set detection limit.

It is seen in the flux residual plot that the ring signature is prominent (above the 100 ppm detection limit) for time-sampling below 15 minutes. This confirms the photometric result from Barnes and Fortney (2004) that the detection of large rings require ∼15 min time-sampling. However, the best photometric results are gotten with time-sampling between 1 - 7 mins where the 70 min ring signature is well sampled. This is within the time-resolution of the upcoming instrument *CHEOPS*[1]. The ring signature is fairly constant below 7 mins time-sampling indicating that 7 mins suffices for the ring detection. The precision of *CHEOPS* in 7 mins is 56 ppm (for 9th magnitude star) which will allow the detection of even low amplitude ring signatures. A time-sampling of 3.5 mins will be required for orientations where the ring signature has a short duration.

At 15 minute time-sampling, the RV ring signature is well above the 1 m/s detection limit. 1 m/s is noted as the current RV precision of *HARPS*[2] (Mayor et al., 2003). This is very promising for the spectroscopic search for rings since RV measurements

[1]CHaracterising ExOPlanet Satellite. *CHEOPS* will have photon noise limited precision of 150 ppm/min for transit across a G5 dwarf star of V=9 magnitude (Broeg et al., 2013).

[2]High Accuracy Radial velocity Planet Searcher

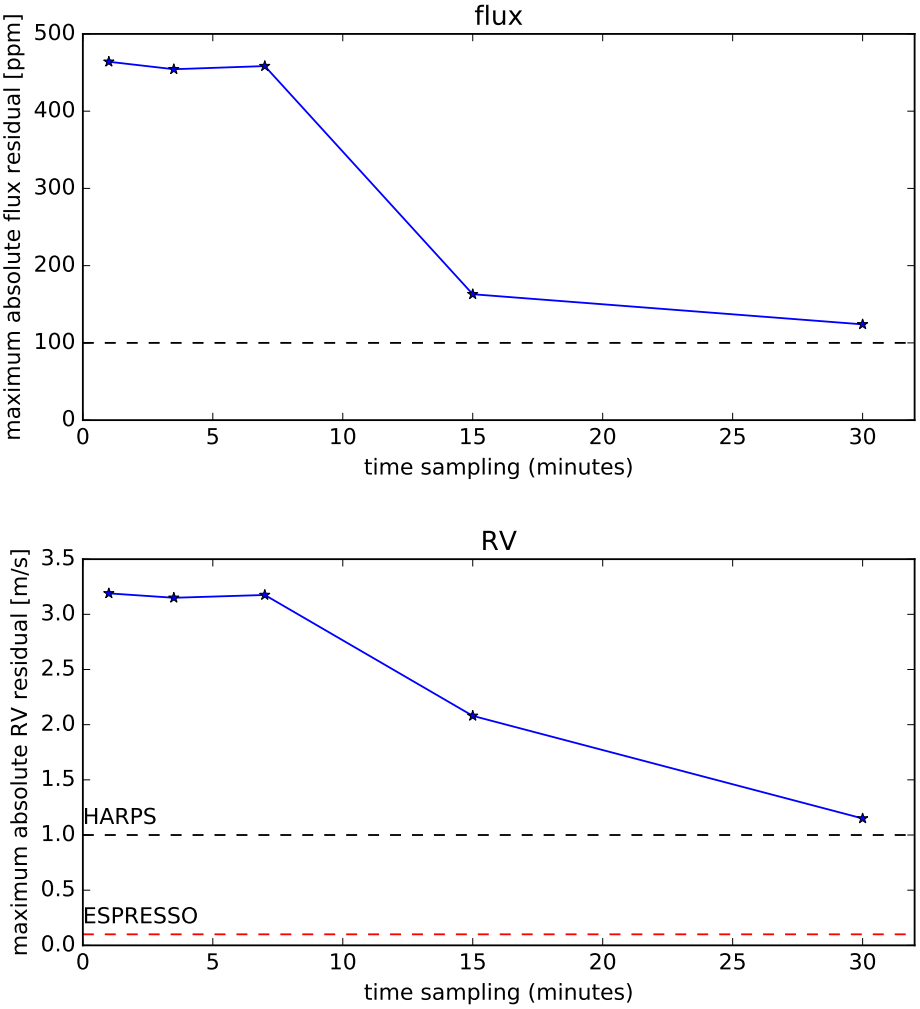

FIGURE 5.7: Top pane: Amplitude of photometric ring signature for different time-sampling. Black line indicates the detection limit of 100 ppm. Bottom pane: Amplitude of spectroscopic ring signature for different time-sampling. Black and Red dashed line indicate detection limit of HARPS (1 m/s) and ESPRESSO (0.1 m/s).

typically require up to ∼15 min integration to average out the short-period stellar oscillations on FGK stars. In addition, upcoming spectrographs like *HIRES* on E-ELT (Marconi et al., 2016) and *ESPRESSO*[3] on VLT will present interesting possibilities for ring detection. For instance, *ESPRESSO* will be capable of 0.1 m/s accuracy on 5th magnitude stars in 1 min exposures (Pepe et al., 2014). Although the typical ∼15 min RV exposure might preclude a 1 min time-sampling, the unprecedented accuracy will increase ring detectability. The *ESPRESSO* detection limit of 0.1 m/s is also shown in the bottom plot of Fig. 5.7. However, it is not clear if this sort of RV precision can be

[3]Echelle SPectrograph for RockyExoplanets and Stable Spectroscopic Observations

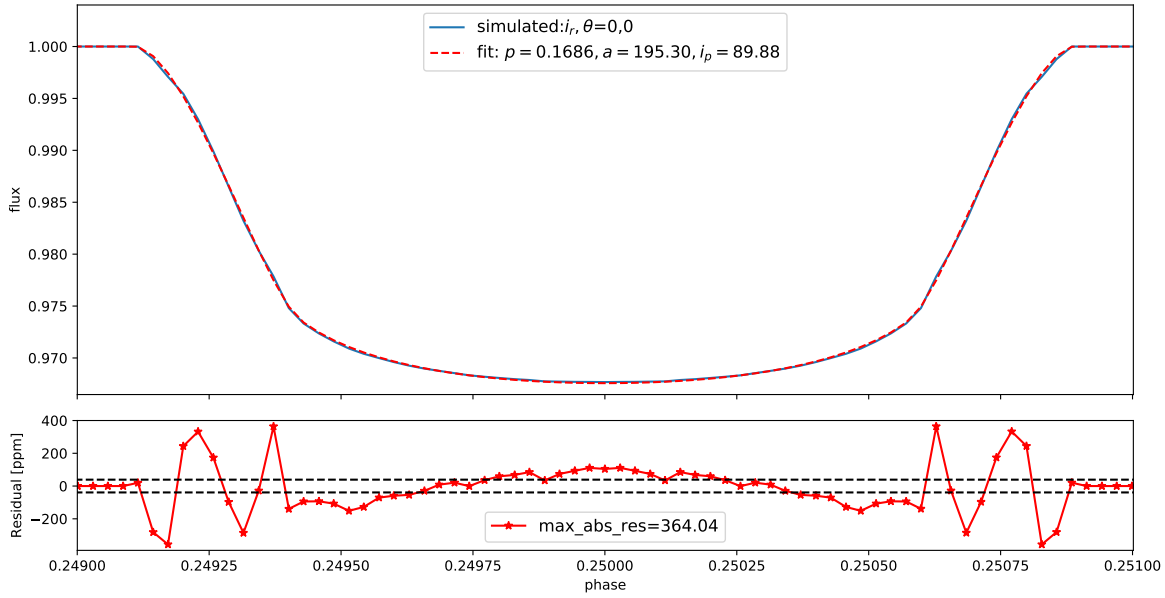

FIGURE 5.8: Top:Light curve fit of the fiducial planet at 1 AU with time sampling of 15 mins. Bottom: Residuals and the *CHEOPS* 39 ppm precision in 15 mins is shown as black dotted lines.

achieved for G and K stars due to stellar granulation and oscillation noise (Dumusque et al., 2011).

The duration of the ring signature depends on semi-major axis, so for the same ringed planet but with a semi-major axis of a_{pr}, the duration of ring signature will be $70 \times (a_{pr}/0.16\,\mathrm{AU})^{1/2}$. This implies that it will be easier to detect rings around longer-period planets since the ring signature timescale will be longer and can be sampled more easily. For instance, the same ringed planet at 1 AU will have ring signature timescale of 175 mins. The resulting light-curve can still be well-sampled with 15 min exposure time for ring detection and a photometric precision of 39 ppm (V=9 star) will be achieved with *CHEOPS* (Fig. 5.8). The RM signal can be sampled with up to 20 min exposure with *ESPRESSO* RV precision of 0.1 m/s for V=8.6 star (Fig. 5.9). The impact parameter, planet radius and ring parameters can also alter the duration of the ring signature.

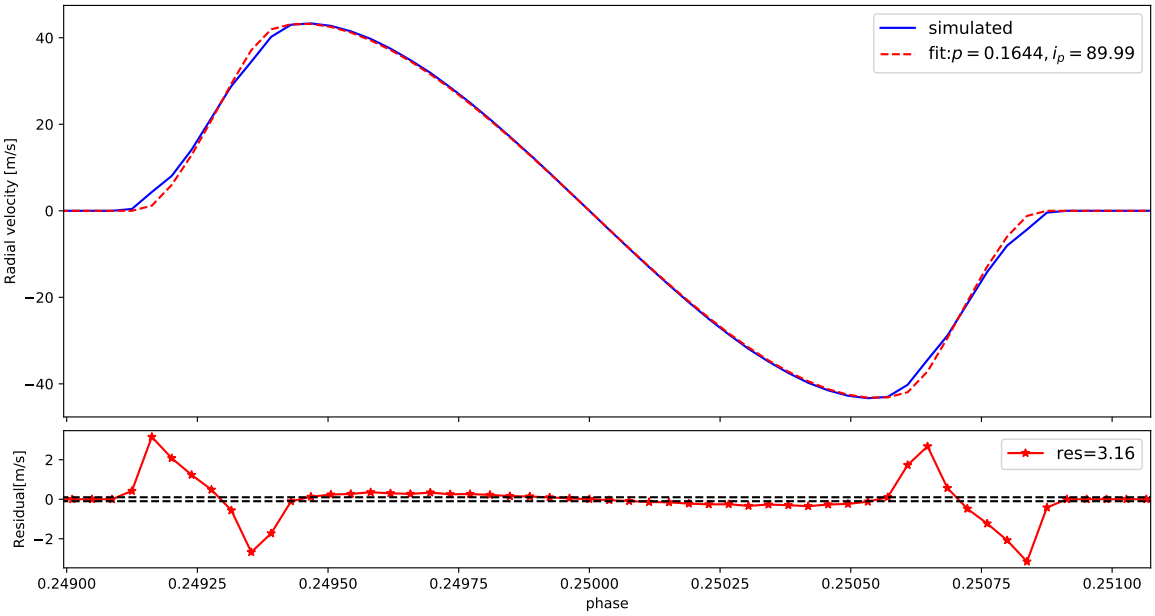

FIGURE 5.9: Top:RM signal fit of the fiducial planet at 1 AU with time sampling of 20 mins. Bottom: Residuals and the *ESPRESSO* 0.1 m/s precision is shown as black dotted lines.

Chapter 6

Conclusions

This work presented the development of SOAP3.0 and demonstrated its capability for the simulation of photometric and spectroscopic signal of a transiting ringed planet. SOAP3.0 is able to generate the light-curves and RM signals of a planet with the additional effects of rings included. The suitability of this tool was validated by comparing its result with others in literature. The tool was used to characterise ring signatures considering different possible orientations of the ring and it highlighted the ring orientations that are favorable for detection using each of the transit techniques. Most interesting are the orientations close to edge-on for which ring signatures can still be detected. This is very promising in the search for exoplanetary rings and the characterisation sheds important light as to how rings might be detected around exoplanets if they exist as expected.

The work highlighted different factors that would impact both methods either to amplify or attenuate the ring signature. It was observed that:

- The gap between planet surface and ring inner radius is pertinent for ring detection.
- High impact parameter transits cause asymmetry in the signals which leads to large ring signatures for tilted rings.
- Transits across fast rotating stars can have more prominent spectroscopic ring signatures than in the photometry.

- Inaccurate estimation of the limb darkening coefficients leads to damping of ring signatures more in the spectroscopic RM signals than in the photometric light-curves.

- Time-sampling $\leq$7 minutes is required for the photometric ring detection while 15 minute sampling suffices for spectroscopic ring detection.

- The precision of upcoming instruments like *ESPRESSO* and *CHEOPS* will increase the ring detectability.

It should be noted that although we considered the tough scenario of a ringed planet orbiting at 0.16 AU, the method is valid for planets at any distance from the star with the only difference being in the timescale. Our results have thus shown the complementarity of the two transit techniques, a synergy which will increase the certainty of any positive ring detection.

The result of the work has been submitted to the Astronomy & Astrophysics journal and accepted for publication. Future development will be to apply the ring model presented here to search for rings in transit data. The ideal targets for this search would be:

- Transit candidates that have been classified as false-positives on the account of large transit depths.

- Transit candidates with V-shaped light-curves (since they are mostly flagged as false positives).

- Confirmed planets with anomalously low densities.

- Transiting planets for which the transit derived stellar density is low and is in disagreement with that derived using asteroseismology.

Bibliography

Addison, B. C. et al. (2016). "Spin–orbit Alignment for Three Transiting Hot Jupiters: WASP-103b, WASP-87b, and WASP-66b". In: *The Astrophysical Journal* 823.1, p. 29. URL: http://stacks.iop.org/0004-637X/823/i=1/a=29.

Aizawa, Masataka et al. (2017). "Toward Detection of Exoplanetary Rings via Transit Photometry: Methodology and a Possible Candidate". In: *The Astronomical Journal* 153.4, p. 193. URL: http://stacks.iop.org/1538-3881/153/i=4/a=193.

Anderson, D. R. et al. (2010). "Wasp-17b: An Ultra-Low Density Planet in a Probable Retrograde Orbit". In: *The Astrophysical Journal* 709.1, p. 159. URL: http://stacks.iop.org/0004-637X/709/i=1/a=159.

Barnes, Jason W. and Jonathan J. Fortney (2003). "Measuring the Oblateness and Rotation of Transiting Extrasolar Giant Planets". In: *The Astrophysical Journal* 588.1, p. 545. URL: http://stacks.iop.org/0004-637X/588/i=1/a=545.

— (2004). "Transit Detectability of Ring Systems around Extrasolar Giant Planets". In: *The Astrophysical Journal* 616.2, p. 1193. URL: http://stacks.iop.org/0004-637X/616/i=2/a=1193.

Barros, S. C. C. et al. (2012). "High-precision transit observations of the exoplanet WASP-13b with the RISE instrument". In: *Monthly Notices of the Royal Astronomical Society* 419.2, p. 1248. DOI: 10.1111/j.1365-2966.2011.19784.x. eprint: /oup/backfile/content_public/journal/mnras/419/2/10.1111/j.1365-2966.2011.19784.x/2/mnras0419-1248.pdf. URL: +http://dx.doi.org/10.1111/j.1365-2966.2011.19784.x.

Boisse, I., X. Bonfils, and N. C. Santos (2012). "SOAP. A tool for the fast computation of photometry and radial velocity induced by stellar spots". In: *Aap* 545, A109, A109. DOI: 10.1051/0004-6361/201219115. arXiv: 1206.5493 [astro-ph.IM].

Boué, G. et al. (2013). "New analytical expressions of the Rossiter-McLaughlin effect adapted to different observation techniques". In: *aap* 550, A53, A53. DOI: 10.1051/0004-6361/201220146. arXiv: 1211.3310 [astro-ph.EP].

Broeg, C. et al. (2013). "CHEOPS: A transit photometry mission for ESA's small mission programme". In: *European Physical Journal Web of Conferences*. Vol. 47. European Physical Journal Web of Conferences, p. 03005. DOI: 10.1051/epjconf/20134703005. arXiv: 1305.2270 [astro-ph.EP].

Brown, Timothy M. et al. (2001). "Hubble Space Telescope Time-Series Photometry of the Transiting Planet of HD209458". In: *The Astrophysical Journal* 552.2, p. 699. URL: http://stacks.iop.org/0004-637X/552/i=2/a=699.

Carter, Joshua A. and Joshua N. Winn (2010a). "Empirical Constraints on the Oblateness of an Exoplanet". In: *The Astrophysical Journal* 709.2, p. 1219. URL: http://stacks.iop.org/0004-637X/709/i=2/a=1219.

— (2010b). "The Detectability of Transit Depth Variations Due to Exoplanetary Oblateness and Spin Precession". In: *The Astrophysical Journal* 716.1, p. 850. URL: http://stacks.iop.org/0004-637X/716/i=1/a=850.

Charbonneau, D. et al. (2002). "Detection of an Extrasolar Planet Atmosphere". In: *Apj* 568, pp. 377–384. DOI: 10.1086/338770. eprint: astro-ph/0111544.

Charnoz, Sébastien et al. (2009). "Origin and Evolution of Saturn's Ring System". In: *Saturn from Cassini-Huygens*. Ed. by Michele K. Dougherty, Larry W. Esposito, and Stamatios M. Krimigis. Dordrecht: Springer Netherlands, pp. 537–575. ISBN: 978-1-4020-9217-6. DOI: 10.1007/978-1-4020-9217-6_17. URL: http://dx.doi.org/10.1007/978-1-4020-9217-6_17.

Claret, A. and S. Bloemen (2011). "Gravity and limb-darkening coefficients for the Kepler, CoRoT, Spitzer, uvby, UBVRIJHK, and Sloan photometric systems". In: *aap* 529, A75, A75. DOI: 10.1051/0004-6361/201116451.

Csizmadia, Sz. et al. (2013). "The effect of stellar limb darkening values on the accuracy of the planet radii derived from photometric transit observations". In: *A&A* 549, A9. DOI: 10.1051/0004-6361/201219888. URL: https://doi.org/10.1051/0004-6361/201219888.

Deming, D. et al. (2005). "Infrared radiation from an extrasolar planet". In: *Nature* 434, pp. 740–743. DOI: 10.1038/nature03507. eprint: astro-ph/0503554.

Dumusque, X. et al. (2011). "Planetary detection limits taking into account stellar noise. I. Observational strategies to reduce stellar oscillation and granulation effects". In: *aap* 525, A140, A140. DOI: 10.1051/0004-6361/201014097. arXiv: 1010.2616 [astro-ph.EP].

Dumusque, X., I. Boisse, and N. C. Santos (2014). "SOAP 2.0: A Tool to Estimate the Photometric and Radial Velocity Variations Induced by Stellar Spots and Plages". In: *The Astrophysical Journal* 796.2, p. 132. URL: http://stacks.iop.org/0004-637X/796/i=2/a=132.

Elliot, J. L. et al. (1978). "The radii of Uranian rings alpha, beta, gamma, delta, epsilon, eta, 4, 5, and 6 from their occultations of SAO 158687". In: *Aj* 83, pp. 980–992. DOI: 10.1086/112280.

Endl, Michael et al. (2011). "Kepler-15b: A Hot Jupiter Enriched in Heavy Elements and the First Kepler Mission Planet Confirmed with the Hobby-Eberly Telescope". In: *The Astrophysical Journal Supplement Series* 197.1, p. 13. URL: http://stacks.iop.org/0067-0049/197/i=1/a=13.

Estrada, Paul R. and Jeffrey N. Cuzzi (1996). "Voyager Observations of the Color of Saturn's Rings". In: *Icarus* 122.2, pp. 251 –272. ISSN: 0019-1035. DOI: http://dx.doi.org/10.1006/icar.1996.0124. URL: http://www.sciencedirect.com/science/article/pii/S0019103596901244.

Gaudi, B. Scott and Joshua N. Winn (2007). "Prospects for the Characterization and Confirmation of Transiting Exoplanets via the Rossiter-McLaughlin Effect". In: *The Astrophysical Journal* 655.1, p. 550. URL: http://stacks.iop.org/0004-637X/655/i=1/a=550.

Gaudi, B. Scott, Heon-Young Chang, and Cheongho Han (2003). "Probing Structures of Distant Extrasolar Planets with Microlensing". In: *The Astrophysical Journal* 586.1, p. 527. URL: http://stacks.iop.org/0004-637X/586/i=1/a=527.

Gillon, M. et al. (2017). "Seven temperate terrestrial planets around the nearby ultracool dwarf star TRAPPIST-1". In: *Nature* 542, pp. 456–460. DOI: 10.1038/nature21360. arXiv: 1703.01424 [astro-ph.EP].

Goldreich, P. and S. Tremaine (1982). "The dynamics of planetary rings". In: *ARAA* 20, pp. 249–283. DOI: 10.1146/annurev.aa.20.090182.001341.

Hahn, Joseph M. and Joseph N. Spitale (2013). "An N-body Integrator for Gravitating Planetary Rings, and the Outer Edge of Saturn's B Ring". In: *The Astrophysical Journal* 772.2, p. 122. URL: http://stacks.iop.org/0004-637X/772/i=2/a=122.

Hamilton, D. P. and J. A. Burns (1991). "Orbital stability zones about asteroids". In: *Icarus* 92, pp. 118–131. DOI: 10.1016/0019-1035(91)90039-V.

Hartman, J. D. et al. (2012). "HAT-P-39b–HAT-P-41b: Three Highly Inflated Transiting Hot Jupiters". In: *The Astronomical Journal* 144.5, p. 139. URL: http://stacks.iop.org/1538-3881/144/i=5/a=139.

Heising, Matthew Z., Geoffrey W. Marcy, and Hilke E. Schlichting (2015). "A Search for Ringed Exoplanets Using Kepler Photometry". In: *The Astrophysical Journal* 814.1, p. 81. URL: http://stacks.iop.org/0004-637X/814/i=1/a=81.

Hubbard, W. B. et al. (1985). "Results from observations of the 15 June 1983 occultation by the Neptune system". In: *Aj* 90, pp. 655–667. DOI: 10.1086/113772.

Huber, D. et al. (2013). "Fundamental Properties of Kepler Planet-candidate Host Stars using Asteroseismology". In: *Apj* 767, 127, p. 127. DOI: 10.1088/0004-637X/767/2/127. arXiv: 1302.2624 [astro-ph.SR].

Kenworthy, M. A. and E. E. Mamajek (2015). "Modeling Giant Extrasolar Ring Systems in Eclipse and the Case of J1407b: Sculpting by Exomoons?" In: *The Astrophysical Journal* 800.2, p. 126. URL: http://stacks.iop.org/0004-637X/800/i=2/a=126.

Kipping, D. M. (2014). "Characterizing distant worlds with asterodensity profiling". In: *MNRAS* 440, pp. 2164–2184. DOI: 10.1093/mnras/stu318. arXiv: 1311.1170 [astro-ph.EP].

Lecavelier des Etangs, A. et al. (2017). "Search for rings and satellites around the exoplanet CoRoT-9b using Spitzer photometry". In: *ArXiv e-prints*. arXiv: 1705.01836 [astro-ph.EP].

Lissauer, J. J. and I. de Pater (2013). *Fundamental Planetary Science*.

Madhusudhan, N. et al. (2014). "H_2O Abundances in the Atmospheres of Three Hot Jupiters". In: *Apjl* 791, L9, p. L9. DOI: 10.1088/2041-8205/791/1/L9. arXiv: 1407.6054 [astro-ph.EP].

Mamajek, Eric E. et al. (2012). "Planetary Construction Zones in Occultation: Discovery of an Extrasolar Ring System Transiting a Young Sun-like Star and Future Prospects for Detecting Eclipses by Circumsecondary and Circumplanetary Disks". In: *The Astronomical Journal* 143.3, p. 72. URL: http://stacks.iop.org/1538-3881/143/i=3/a=72.

Mandel, Kaisey and Eric Agol (2002). "Analytic Light Curves for Planetary Transit Searches". In: *The Astrophysical Journal Letters* 580.2, p. L171. URL: http://stacks.iop.org/1538-4357/580/i=2/a=L171.

Marconi, A. et al. (2016). *EELT-HIRES the high-resolution spectrograph for the E-ELT*. DOI: 10.1117/12.2231653. URL: http://dx.doi.org/10.1117/12.2231653.

Mayor, M. and D. Queloz (1995). "A Jupiter-mass companion to a solar-type star". In: *Nature* 378, pp. 355–359. DOI: 10.1038/378355a0.

Mayor, M. et al. (2003). "Setting New Standards with HARPS". In: *The Messenger* 114, pp. 20–24.

McLaughlin, D. B. (1924). "Some results of a spectrographic study of the Algol system." In: *Apj* 60. DOI: 10.1086/142826.

Miner, E. D., R.R. Wessen, and J.N. Cuzzi (2007). *Planetary Ring Systems*.

Neilson, H. R. et al. (2017). "Limb Darkening and Planetary Transits: Testing Center-to-limb Intensity Variations and Limb-Darkening Directly from Model Stellar Atmospheres". In: *ArXiv e-prints*. arXiv: 1704.07376 [astro-ph.EP].

Neto, E. Vieira and O. C. Winter (2001). "Time Analysis for Temporary Gravitational Capture: Satellites of Uranus". In: *The Astronomical Journal* 122.1, p. 440. URL: http://stacks.iop.org/1538-3881/122/i=1/a=440.

Nicholson, Philip D. et al. (2008). "A close look at Saturn's rings with Cassini VIMS". In: *Icarus* 193.1, pp. 182 –212. ISSN: 0019-1035. DOI: http://dx.doi.org/10.1016/j.icarus.2007.08.036. URL: http://www.sciencedirect.com/science/article/pii/S0019103507003491.

Ohta, Y., A. Taruya, and Y. Suto (2009). "Predicting Photometric and Spectroscopic Signatures of Rings Around Transiting Extrasolar Planets". In: *Apj* 690, pp. 1–12. DOI: 10.1088/0004-637X/690/1/1. eprint: astro-ph/0611466.

Ohta, Yasuhiro, Atsushi Taruya, and Yasushi Suto (2005). "The Rossiter-McLaughlin Effect and Analytic Radial Velocity Curves for Transiting Extrasolar Planetary Systems". In: *The Astrophysical Journal* 622.2, p. 1118. URL: http://stacks.iop.org/0004-637X/622/i=2/a=1118.

Oshagh, M. et al. (2013). "SOAP-T: a tool to study the light curve and radial velocity of a system with a transiting planet and a rotating spotted star". In: *aap* 549, A35, A35. DOI: 10.1051/0004-6361/201220173. arXiv: 1211.1311 [astro-ph.EP].

Oshagh, M. et al. (2016). "Can stellar activity make a planet seem misaligned?" In: *aap* 593, A25, A25. DOI: 10.1051/0004-6361/201628728. arXiv: 1607.03134 [astro-ph.EP].

Pepe, F. et al. (2014). "ESPRESSO: The next European exoplanet hunter". In: *Astronomische Nachrichten* 335.1, pp. 8–20. ISSN: 1521-3994. DOI: 10.1002/asna.201312004. URL: http://dx.doi.org/10.1002/asna.201312004.

Perryman, M. (2011). *The Exoplanet Handbook*.

Rossiter, R. A. (1924). "On the detection of an effect of rotation during eclipse in the velocity of the brigher component of beta Lyrae, and on the constancy of velocity of this system." In: *Apj* 60. DOI: 10.1086/142825.

Sanchis-Ojeda, Roberto and Joshua N. Winn (2011). "Starspots, Spin-Orbit Misalignment, and Active Latitudes in the HAT-P-11 Exoplanetary System". In: *The Astrophysical Journal* 743.1, p. 61. URL: http://stacks.iop.org/0004-637X/743/i=1/a=61.

Santos, N. C. et al. (2015). "Detecting ring systems around exoplanets using high resolution spectroscopy: the case of 51 Pegasi b". In: *aap* 583, A50, A50. DOI: 10.1051/0004-6361/201526673. arXiv: 1509.00723 [astro-ph.EP].

Schlichting, Hilke E. and Philip Chang (2011). "Warm Saturns: On the Nature of Rings around Extrasolar Planets That Reside inside the Ice Line". In: *The Astrophysical Journal* 734.2, p. 117. URL: http://stacks.iop.org/0004-637X/734/i=2/a=117.

Schneider, Jean (1999). "The study of extrasolar planets: methods of detection, first discoveries and future perspectives". In: *Comptes Rendus de l'Académie des Sciences - Series IIB - Mechanics-Physics-Astronomy* 327.6, pp. 621 –634. ISSN: 1287-4620. DOI: http://dx.doi.org/10.1016/S1287-4620(99)80093-3. URL: http://www.sciencedirect.com/science/article/pii/S1287462099800933.

Seager, S. and G. Mallén-Ornelas (2003). "A Unique Solution of Planet and Star Parameters from an Extrasolar Planet Transit Light Curve". In: *The Astrophysical Journal* 585.2, p. 1038. URL: http://stacks.iop.org/0004-637X/585/i=2/a=1038.

Sing, D. K. (2010). "Stellar limb-darkening coefficients for CoRot and Kepler". In: *aap* 510, A21, A21. DOI: 10.1051/0004-6361/200913675. arXiv: 0912.2274 [astro-ph.EP].

Soderblom, D. R. (2010). "The Ages of Stars". In: *ARAA* 48, pp. 581–629. DOI: 10.1146/annurev-astro-081309-130806. arXiv: 1003.6074 [astro-ph.SR].

Tusnski, Luis Ricardo M. and Adriana Valio (2011). "Transit Model of Planets with Moon and Ring Systems". In: *The Astrophysical Journal* 743.1, p. 97. URL: http://stacks.iop.org/0004-637X/743/i=1/a=97.

Zhu, Wei et al. (2014). "Constraining the Oblateness of Kepler Planets". In: *The Astrophysical Journal* 796.1, p. 67. URL: http://stacks.iop.org/0004-637X/796/i=1/a=67.

Zuluaga, Jorge I. et al. (2015). "A Novel Method for Identifying Exoplanetary Rings". In: *The Astrophysical Journal Letters* 803.1, p. L14. URL: http://stacks.iop.org/2041-8205/803/i=1/a=L14.